



UNIVERSITY OF HELSINKI

<https://helda.helsinki.fi>

Single-Cell RNA Sequencing-Based Characterization of Resident Lung Mesenchymal Stromal Cells in Bronchopulmonary Dysplasia

Mizikova, Ivana; Lesage, Flore; Cyr-Depauw, Chanele; Cook, David P.; Hurskainen, Maria ...

2022-05-27

Oxford University Press

<http://hdl.handle.net/10138/358136>

Mizikova, I, Lesage, F, Cyr-Depauw, C, Cook, D P, Hurskainen, M, Hänninen, S M, Vadivel, A, Bardin, P, Zhong, S, Carpen, O, Vanderhyden, B C & Thebaud, B 2022, 'Single-Cell RNA Sequencing-Based Characterization of Resident Lung Mesenchymal Stromal Cells in Bronchopulmonary Dysplasia', *Stem Cells*, vol. 40, no. 5, pp. 479-492. <https://doi.org/10.1093/stmcls/sxab023>

Downloaded from Helda, University of Helsinki institutional repository. <https://helda.helsinki.fi>
This is an electronic reprint of the original article.
This reprint may differ from the original in pagination and typographic detail.
Please cite the original version.

1 **Single-cell RNA sequencing-based characterization of resident lung**
2 **mesenchymal stromal cells in bronchopulmonary dysplasia**

3 I. Mižiková^{1,2}, F. Lesage^{1,2}, C. Cyr-Depauw^{1,2}, D. P. Cook^{2,3}, M. Hurskainen^{1,2,4,5}, S.M.
4 Hänninen⁶, A. Vadivel¹, P. Bardin^{1,2}, S. Zhong¹, O. Carpen⁶, B. C. Vanderhyden^{2,3,8}, B.
5 Thébaud^{1,2,7}

6

7 ¹ Sinclair Centre for Regenerative Medicine, Ottawa Hospital Research Institute, Ottawa, ON,
8 Canada

9 ² Department of Cellular and Molecular Medicine, University of Ottawa, Ottawa, Ontario,
10 Canada

11 ³ Cancer Therapeutics Program, Ottawa Hospital Research Institute, Ottawa, Ontario, Canada

12 ⁴ Division of Pediatric Cardiology, New Children's Hospital, Helsinki University Hospital and
13 University of Helsinki, Helsinki, Finland

14 ⁵ Pediatric Research Center, New Children's Hospital, University of Helsinki and Helsinki
15 University Hospital, Helsinki, Finland

16 ⁶ Precision Cancer Pathology, Department of Pathology and Research Program in Systems
17 Oncology, University of Helsinki and HUS Diagnostic Center, Helsinki University Hospital,
18 Helsinki, Finland

19 ⁷ Department of Pediatrics, Children's Hospital of Eastern Ontario (CHEO) and CHEO Research
20 Institute, University of Ottawa, Ottawa, Ontario, Canada

21 ⁸ Department of Obstetrics and Gynecology, University of Ottawa/The Ottawa Hospital, Ottawa,
22 Ontario, Canada

23

24 Running head: Lung MSCs in BPD.

25

26

27 **ABSTRACT (limit 250 words)**

28 Late lung development is a period of alveolar and microvascular formation, which is pivotal in
29 ensuring sufficient and effective gas exchange. Defects in late lung development manifest in
30 premature infants as a chronic lung disease named bronchopulmonary dysplasia (BPD).
31 Numerous studies demonstrated the therapeutic properties of exogenous bone marrow and
32 umbilical cord-derived mesenchymal stromal cells (MSCs) in experimental BPD. However, very
33 little is known regarding the regenerative capacity of resident lung MSCs (L-MSCs) during
34 normal development and in BPD. In this study we aimed to characterize the L-MSC population
35 in homeostasis and upon injury. We used single-cell RNA sequencing (scRNA-seq) to profile *in*
36 *situ* *Ly6a*⁺ L-MSCs in the lungs of normal and O₂-exposed neonatal mice (a well-established
37 model to mimic BPD) at three developmental timepoints (postnatal days 3, 7 and 14). Hyperoxia
38 exposure increased the number, and altered the expression profile of L-MSCs, particularly by
39 increasing the expression of multiple pro-inflammatory, pro-fibrotic, and anti-angiogenic genes.
40 In order to identify potential changes induced in the L-MSCs transcriptome by storage and
41 culture, we profiled 15,000 *Ly6a*⁺ L-MSCs after *in vitro* culture. We observed great differences
42 in expression profiles of *in situ* and cultured L-MSCs, particularly those derived from healthy
43 lungs. Additionally, we have identified the location of L-MSCs in the developing lung and
44 propose *Serpinf1* as a novel, culture-stable marker of L-MSCs. Finally, cell communication
45 analysis suggests inflammatory signals from immune and endothelial cells as main drivers of
46 hyperoxia-induced changes in L-MSCs transcriptome.

47 1. INTRODUCTION

48 Late lung development represents an important period in lung maturation marked by an
49 exponential increase in the gas exchange surface area by forming the most distal respiratory
50 units, the alveoli. Within these units, respiration takes place across a thin (0.2 - 2 μ m) alveolo-
51 capillary barrier. Formation of alveolar structures, a process known as alveolarization, is
52 facilitated by spatially and temporarily coordinated interactions between diverse cell types and
53 the pulmonary microenvironment [1]. Defects in late lung development in humans manifest as
54 bronchopulmonary dysplasia (BPD), a multifactorial disease occurring as a consequence of
55 premature birth, respiratory distress, and associated treatments in neonatal intensive care. BPD is
56 the most common chronic disease in children and a leading cause of death in children under the
57 age of 5 [1,2]. BPD is also associated with neurodevelopmental delay, increased incidence of
58 asthma, re-hospitalizations and early-onset emphysema [3,4].

59 To date, multiple studies have demonstrated the lung protective effects of exogenous,
60 bone marrow (BM)- or umbilical cord (UC)-derived, mesenchymal stromal cells (MSCs) in
61 experimental BPD models [5–10]. The discovery of lung resident (L-)MSCs prompted questions
62 regarding the apparent insufficient regenerative capacity of L-MSCs in lung injury [11].
63 Characterizing the L-MSC population in homeostasis and upon injury is pivotal in understanding
64 the apparent contradiction between the therapeutic effects of exogenous MSCs, while the
65 resident population fails to prevent neonatal lung injury from occurring. However, very little is
66 currently known about the role of L-MSCs in postnatal lung development and in BPD. Lung
67 stromal cells, including lipofibroblasts, myofibroblasts and matrix fibroblasts are a potent source
68 of inter-cellular signaling and are known to play an important role in BPD pathogenesis [12].
69 However, how L-MSCs communicate with other cell populations and contribute to the
70 development of BPD remains unknown.

71 While most authors report that L-MSCs can differentiate, to some extent, into
72 chondroblasts, osteoblasts and adipocytes [13], form colonies *in vitro* [13,14], and express
73 classical MSC markers THY1 (CD90), NT5E (CD73) and ENG (CD105) [13,15], no L-MSC-
74 specific marker has yet been established. Due to the lack of standardization for L-MSC
75 identification, as well as differences in expression profiles between species, no single marker has
76 been broadly accepted. Lung mesenchymal progenitor cell markers have been proposed [13,15–

77 18], including LY6A, often referred to as SCA-1 (Stem cell antigen 1) [16–19]. LY6A was
78 proposed as a defining progenitor marker for mesenchymal cell lineages in the lung [19] and
79 LY6A⁺ mesenchymal lung cells were shown to promote colony formation, proliferation and
80 differentiation of epithelial progenitor cells [20].

81 In the study presented here we identify, for the first time, the transcriptome of *Ly6a*⁺ L-
82 MSCs in healthy and diseased developing mouse lungs. We hypothesized, that O₂-exposure (a
83 well-established model to mimic BPD) significantly impacts the phenotype and function of L-
84 MSCs, as well as cellular communication between L-MSCs and other cell populations in the
85 developing lung. We identify perturbations to the phenotype and functional properties of L-
86 MSCs in this model. Furthermore, we report extensive single-cell RNA sequencing (scRNA-seq)
87 profiling of L-MSCs in the lungs of 36 healthy and O₂-exposed mice at three developmental
88 timepoints (P3, P7, and P14). Finally, we investigate cultured *Ly6a*⁺ L-MSCs and *Ly6a*⁻ mouse
89 lung stromal cells by scRNA-seq. We identify changes in L-MSCs transcription profile induced
90 by storage and culture and present novel, culture-stable marker for this rare progenitor
91 population.

92 2. MATERIALS AND METHODS

93 2.1 Experimental animals

94 Pregnant C57BL/6N mice were purchased from Charles Rivers Laboratories, Saint Constant,
95 QC, Canada at embryonic day (E)15. Mice were housed by the Animal Care and Veterinary
96 Service of the University of Ottawa in accordance with institutional guidelines. All study
97 protocols were approved by the animal ethics and research committee of the University of
98 Ottawa (protocol OHRI-1696) and conducted according to guidelines from the Canadian Council
99 on Animal Care (CCAC). Mouse pups born on the same day, were randomized at the day of birth
100 [postnatal day (P)0] and divided into equal-sized litters of 6-8 pups/cage. Cages were then
101 maintained either in room air (normoxia, 21% O₂), or in normobaric hyperoxia (85% O₂) until
102 the day of harvest. The hyperoxic environment was maintained in sealed plexiglass chambers
103 with continuous oxygen monitoring (BioSpherix, Redfield, NY). Mice were maintained in 12/12
104 hours light/dark cycle and received food ad libidum. In order to avoid confounding factors
105 associated with oxygen toxicity, nursing dams were rotated between normoxic and hyperoxic
106 group every 48 hours. Euthanasia was performed by an intraperitoneal (i.p.) injection of 10 µl/g
107 Pentobarbital Sodium (CDMV, Saint-Hyacinthe, QC, Canada).

108

109 2.2 Lung isolation

110 Mouse pups designated for mean linear intercept (MLI) assessment or fluorescent in situ
111 hybridization (FISH) were euthanized at P7 and P14, respectively. Following euthanasia, the
112 chest was opened, mice were tracheotomized and lungs were installation-fixed for 5 minutes at
113 20cm H₂O hydrostatic pressure. Lungs designated for histological assessment were fixed with
114 1.5% (w/v) paraformaldehyde (PFA) (Sigma-Aldrich, Oakville, ON, Canada) and 1.5% (w/v)
115 glutaraldehyde (Sigma-Aldrich, Oakville, ON, Canada) in 150mM HEPES (Sigma-Aldrich,
116 Oakville, ON, Canada). Lungs designated for FISH were fixed with 4% (w/v) PFA (Sigma-
117 Aldrich, Oakville, ON, Canada). In both instances, lungs were kept in the fixation solution for 48
118 hours at 4°C and collected for embedding in paraffin. Paraffin-embedded tissue blocks
119 designated for histological analyses were sectioned at 3 or 4µm as needed. Tissue dehydration,
120 paraffin embedding and sectioning were performed by the University of Ottawa Louise Pelletier
121 Histology Core Facility.

122 Mouse pups designated for lung cells isolation and fluorescence activated cell sorting
123 (FACS) analyses were euthanized at P7. Mice also received an i.p. injection of 10 mU/g Heparin
124 Sodium (LEO Pharma INC., Thornhill, ON, Canada). Following euthanasia, the chest was
125 opened and the left atrium was perforated. Lungs were perfused through the right ventricle with
126 5 ml of 25 U/ml Heparin Sodium in DPBS supplemented with Mg^{2+}/Ca^{2+} (ThermoFisher
127 Scientific, Burlington, ON, Canada) until white. Lungs were removed from the thoracic cavity,
128 dissected into individual lobes, and digested in enzyme mix at 37°C by gentleMACS™ Octo
129 Dissociator (Miltenyi Biotech, Bergisch Gladbach, Germany). The detailed procedure, as well as
130 enzyme mixture contents are provided in Supplementary Method S1. The suspension was then
131 centrifuged and the resulting pellet was washed with 5 ml of 5% FBS (Sigma-Aldrich, Oakville,
132 ON, Canada) in 1× DPBS (Lonza, Basel, Switzerland), filtered through 70 µm filter (Corning
133 Life Sciences, Tewksbury, MA, USA) and centrifuged again. The resulting pellet was
134 resuspended in 1ml of cold RBC lysis buffer (ThermoFisher Scientific, Burlington, ON, Canada)
135 for 3 minutes at room temperature (RT). The cell suspension was then diluted with 5ml of 5%
136 FBS solution, centrifuged and washed twice.

137 A detailed flowchart illustrating the allocation of each mice to respective experimental
138 groups is depicted in Supplementary figure 1.

139

140 **2.3 Mean linear intercept (MLI) measurement**

141 Paraffin-embedded tissue blocks were sectioned at 4µm, stained with hematoxylin and eosin
142 (H&E) stain, and scanned using the Axio Scan.Z1 (Zeiss, Oberkochen, Germany). The mean
143 linear intercept (MLI) was estimated with Fiji/ImageJ software using a 64-point grid as described
144 previously [21]. A total of 20 randomly selected 500µm×500µm fields of view were assessed in
145 each lung.

146

147 **2.4 Fluorescent activated cell sorting (FACS)**

148 The number of cells in the single-cell suspension was estimated using the EVE NanoEnTek
149 automatic cell counter and a total of 1×10^6 cells/sample were resuspended in 550 µl of FACS
150 buffer (5% (v/v) FBS and 1mM EDTA in 1×DPBS). Cells were then incubated at RT in the dark

151 with 2 $\mu\text{l}/1\times 10^6$ cells of CD16/32 antibody for 15 minutes. Following blocking, cells were
152 centrifuged and pellets were resuspended in 1:100 mixture of panel of antibodies: FITC-CD31,
153 AF647-CD45, Pe/Cy7- CD326, and BV421- LY-6A/E (Supplementary table 1). Cells were
154 incubated with antibodies for 20 minutes in dark at RT, pelleted and washed 3x with FACS
155 buffer. FACS was performed immediately using a MoFlo XDP (XDP, Beckman Coulter,
156 Fullerton, CA, USA) and compensation and analysis was done using Summit v.5.4 at the Ottawa
157 Hospital Research Institute (OHRI) StemCore facility.

158

159 **2.5 Cell culture and storage**

160 The detailed procedure is provided in Supplementary Method S2.

161

162 **2.6 Colony formation assay**

163 The detailed procedure is provided in Supplementary Method S3.

164

165 **2.7 MSCs surface marker profiling**

166 Cultured, passage 3 CD31⁻/CD45⁻/EpCAM⁻/LY6A⁺ L-MSCs were profiled for MSC surface
167 markers by flow cytometry. Briefly, 3×10^5 cells/sample were resuspended in 200 μl of FACS
168 buffer in 96-well plate and incubated at RT in the dark with 2 $\mu\text{l}/1\times 10^6$ cells of CD16/32
169 antibody for 15 minutes. Cells were then divided to 3 equal fractions, centrifuged and
170 resuspended in one of the following 1:100 mixture of antibodies: i) BV421-CD31, Pe/Cy7-
171 conjugated CD326, PE-CD73, and AF488- D105; ii) AF647- CD45, BV421-LY-6A/E, PE-
172 conjugated CD34, and AF488-CD146; iii) PB-CD90.2 (Supplementary table 1). Cells were
173 incubated with antibodies for 20 minutes in dark at RT, pelleted and washed 3x with FACS
174 buffer. Flow cytometry was performed immediately using a MoFlo XDP (XDP, Beckman
175 Coulter, Fullerton, CA, USA) and compensation and analysis was done using Summit v.5.4 at
176 the OHRI core facility.

177

178 **2.8 Osteogenic differentiation**

179 The detailed procedure is provided in Supplementary Method S4.

180

181 **2.9 Adipogenic differentiation**

182 The detailed procedure is provided in Supplementary Method S5.

183

184 **2.10 Chondrogenic differentiation**

185 The detailed procedure is provided in Supplementary Method S6.

186

187 **2.11. Fluorescent in situ hybridization**

188 The detailed procedure, as well as a list of used probes are provided in Supplementary Method
189 S7.

190

191 **2.12. Multiplexing samples for scRNA-seq**

192 Multiplexing was performed according to the MULTI-seq protocol [22]. The detailed procedure
193 is provided in Supplementary Method S8.

194

195 **2.13. scRNA-seq library preparation and sequencing**

196 Single-cell suspensions were processed using the 10x Genomics Single Cell 3' v3 RNA-seq kit
197 by Ottawa Hospital Research Institute Stem Core Laboratories. Gene expression libraries were
198 prepared according to the manufacturer's protocol. MULTI-seq barcode libraries were retrieved
199 from the samples and libraries were prepared independently, as described previously[22]. Final
200 libraries were sequenced on the NextSeq500 platform (Illumina) to reach an approximate depth
201 of 20,000-25,000 reads/cell.

202

203 **2.14. scRNA-seq data analyses and quantification**

204 **Processing and demultiplexing**

205 Raw sequencing reads were processed using CellRanger v3.0.2 for lung homogenate sample and
206 v3.1.0 for cultured cells, aligning reads to the mm10 build of the mouse genome. Except for
207 explicitly setting `--expect-cells=25000`, default parameters were used for all samples. MULTI-
208 seq barcode libraries were trimmed prior to demultiplexing to 28bp using Trimmomatic (v0.36).
209 Demultiplexing was performed using the deMULTIplex R package (v1.0.2) as described
210 previously[22,23]. Only cells positive for a single barcode were kept for further analysis and
211 sample annotations were added to all cells in the data set.

212

213 **Quality control, integration, and clustering**

214 All main processing steps were performed with Seurat v.4.0.0[24]. Quality control was
215 performed independently on each library to find appropriate filtering thresholds. Expression
216 matrices were loaded as Seurat objects into R. Only cells with > 200 genes detected and $< 20\%$
217 of UMIs mapped to mitochondrial genes were retained. Each unique sample was split based on
218 MULTI-seq sample barcodes into a separate Seurat object. SCTransform[25] was used to
219 normalize samples, select highly variable genes, and to regress out cell cycle and cell stress
220 effects. To eliminate batch effects or biological variability effects on clustering, the data
221 integration method implemented by Seurat for SCTransform-normalized data was performed,
222 using the `SelectIntegrationFeatures()`, `PrepSCTIntegration()`, `FindIntegrationAnchors()`, and
223 `IntegrateData()` functions. PCA was performed on the top 3000 variable genes and the data was
224 clustered at a low resolution (`dims=1:30`, `resolution=0.2` for lung homogenate data and 0.1 for
225 cultured MSCs) with the Louvain algorithm implemented in the `FindClusters()` function in
226 Seurat. Cell populations were identified with a simple Wilcoxon rank sum test with the
227 `FindAllMarkers()` function in Seurat.

228 In the case of stromal cells from lung homogenates, a previously published, publicly
229 available scRNA-seq dataset from newborn mice was re-analyzed[23]. A novel Ly6a⁺ L-MSc
230 population was identified based on the expression of Ly6a. New cell type labels for stromal
231 populations were then added to the Seurat object containing all data.

232

233 **Differential expression analysis (DSA), gene set enrichment analysis (GSEA) and functional**
234 **enrichment analysis**

235 To identify differentially expressed genes in response to hyperoxia or as a result of mouse age,
236 we used the R package muscat (v1.4.0). Pseudobulk expression profiles were generated for each
237 sample in each cluster and differential expression was tested between groups associated with the
238 experimental conditions. Genes with an adjusted p-value < 0.05 and a detection rate $\geq 10\%$ in at
239 least one of the conditions tested were considered significant. To further identify gene sets
240 associated with differentially expressed genes, we used the R package fgsea (v1.16.0). List of
241 gene sets comprised all GO terms, KEGG pathways, Reactome pathways, and the MSigDB
242 Hallmark gene sets acquired from the Molecular Signatures Database (v7.2)[26]. Gene sets with
243 an adjusted p-value < 0.05 were considered significantly enriched. Normalized enrichment score
244 (NES) was used to assess whether gene sets were associated with upregulated or downregulated
245 genes. Functional enrichment analysis (FEA) for selected ligands produced by Ly6a+ L-MSCs
246 were performed using the online Metascape tool[27]. Summary pathways relevant to lung were
247 considered.

248

249 **Cell communication inference**

250 To explore cell communication networks behind the developmental age, or hyperoxia-specific
251 effects, we utilized the R package nichenetr (v1.0.0), which uses information about expression of
252 cognate ligands, receptors, signaling pathways, and genomic targets to infer cell communication
253 patterns[28]. Differential gene expression analysis for P3 vs. P14, or hyperoxia vs. normoxia
254 groups were used in the NicheNet analysis. To prioritize results, analysis was limited to signaling
255 contributing to the effects in receiver cell types with >200 differentially expressed genes at P14
256 or in response to hyperoxia, but included all cell types as potential ligand senders. Background
257 expression of genes was specified with default approach used in NicheNet's pipeline, using all
258 genes with $>10\%$ detection in a given cluster. While using cells from both experimental
259 conditions, developmental age, or hyperoxia-induced ligands from cell types that increase in
260 proportion with age or in hyperoxia samples were prioritized. For each "receiver" cell

261 population, top 10 ligands predicted to drive developmental age, or hyperoxia-induced responses
262 were selected based on the Pearson correlation coefficient between the ligand-target regulatory
263 potential score of each ligand and the target indicator vector. Further, we assessed whether the
264 expression of ligands and receptors was upregulated, or whether the populations expressing the
265 ligands increased in proportion in P14 or hyperoxia samples, respectively. Finally, potential
266 target genes were inferred. Summaries of ligand-receptor interactions are represented in circos
267 plots.

268

269 **2.15. Statistical analysis**

270 All statistical analyses were performed with GraphPad Prism 8.0. The presence of potential
271 statistical outliers was determined by Grubbs' test. Data are presented as means \pm SD.
272 Differences in case of two-member groups were evaluated either by unpaired Student's *t*-test, or
273 multiple unpaired Student's *t*-test with correction for multiple comparisons using the Holm-
274 Šidák method. P values < 0.05 were considered as significant and depicted as following: P values
275 < 0.05 : *; P values < 0.01 : **; P values < 0.001 : ***; P values < 0.0001 : ****.

276 3. RESULTS

277 3.1 The developing murine lung contains a population of L-MSC marked by the expression 278 of *Ly6a*

279 In order to understand the expression patterns unique to LY6A⁺ L-MSCs in the developing lung,
280 we took advantage of a publicly available scRNA-seq dataset from newborn mice[23]. Within
281 this dataset, we analyzed 7,994 stromal cells from normoxia or hyperoxia-exposed developing
282 mouse pups on postnatal days (P)3, 7, and 14, clustered into 6 distinct populations (Fig. 1A).
283 Based on the expression pattern of commonly used MSC markers (Fig. 1B, Supplementary fig.
284 2A) we selected *Ly6a* as most suitable marker to identify L-MSC in lung stroma. We then
285 subsetting the *Ly6a*⁺ cells, belonging almost exclusively to the *Coll4a1*⁺ fibroblasts, as a separate,
286 seventh cluster (Fig. 1B). Differential gene expression analysis revealed that *Ly6a*⁺ L-MSCs
287 could be characterized by the expression of additional markers, including *Lum*, *Serpinf1*, or *Dcn*,
288 with *Lum* being the single most unique identifier of the population (Fig. 1C, Supplementary table
289 2). It was previously shown to inhibit migration, invasion, and tube-formation in BM-MSCs[29],
290 and was implicated in epithelial-mesenchymal transition and fibrocyte differentiation[30]. While
291 *Ly6a*⁺ L-MSCs expressed additional MSC markers *Mcam*, *Alcam* and *Eng*, their expression did
292 not serve as a reliable indicator of *Ly6a*⁺ L-MSCs (Fig. 1D).

293

294 3.2 The transcription profile and signaling activity of *Ly6a*⁺ L-MSCs change significantly 295 during postnatal lung development

296 We first aimed to understand how the L-MSC population changes in the postnatal developing
297 lung. While the size of the population remained unchanged between P3 and P7, the second week
298 of lung development in healthy mice was associated with an increase in the size of the *Ly6a*⁺
299 stromal population (Figure 1E, Supplementary table 3). Similarly, differential state analysis
300 (DSA) in normally developing lungs revealed that most changes in gene expression occurred in
301 L-MSC between P7 and P14 (Fig. 1F, Supplementary table 4). Although the expression of genes
302 such as *Apoe*, *Inmt*, *Klf9* and *Abca1* was drastically increased in L-MSCs, these genes were also
303 considerably upregulated in *Ly6a*⁻ stromal cells (Supplementary table 4). The largest L-MSC -
304 specific expression changes were observed for *Mmp3*, *C1s1*, *Podn*, *Dlk1*, and *Agtr2* (Fig. 1G).

305 Gene set enrichment analysis (GSEA) identified extracellular matrix (ECM) formation, vascular
306 development, and wound healing among the activated pathways (Fig. 1H, Supplementary table
307 5).

308 Next, to further understand how L-MSCs send and receive signals during postnatal
309 development, we performed a cell communication analysis. We inferred developmental age-
310 induced cellular communications between *Ly6a*⁺ L-MSCs and other lung populations using the
311 NicheNet tool [23,28] (Fig. 2A, Supplementary fig. 3-5, Supplementary table 6). During
312 development L-MSCs received signals from several cell populations, including endothelial cells,
313 interstitial macrophages (Int Mf), alveolar epithelial type 2 (AT2) cells, and stromal cells (Fig.
314 2A). *Col4a1*, *Fat1*, *Hmgb2*, *Vcam1* and *Hc* were identified as most potent ligands, targeting
315 numerous downstream genes in the developing L-MSCs, including *Klf9*, *Top2a* and other
316 strongly de-regulated genes (Fig. 2A-B, Figure 1F, Supplementary table 4). Furthermore, L-
317 MSCs produced numerous ligands, targeting most lung cell populations, including itself (Fig.
318 2A), Among the most broadly acting ligands were *Agt*, *App*, and *ApoE* (Fig. 2C). Functional
319 enrichment analysis (FEA) revealed, that the expression of the L-MSC-produced ligands was
320 associated with pathways related to angiogenesis, cell migration, adhesion and chemotaxis, and
321 ECM organization (Supplementary fig. 2B, Supplementary table 7).

322

323 **3.3 The transcription profile and signaling activity of *Ly6a*⁺ L-MSC change significantly** 324 **during postnatal lung development in response to hyperoxia**

325 Hyperoxia induced an increase in proportion of *Ly6a*⁺ stromal cells as determined by scRNA-seq
326 analysis at P14 (Fig. 1F, Supplementary table 3). This was consistent with increased proportion
327 of LY6A⁺ stromal cells in hyperoxia-exposed lungs at P7 as measured by flow cytometry
328 (Supplementary fig. 2C-D). In order to identify hyperoxia-induced changes in gene expression
329 specific to *Ly6a*⁺ L-MSCs, we performed a DSA for both, *Ly6a*⁺ L-MSC population and non-
330 progenitor *Ly6a*⁻ stromal cells (Supplementary table 8). Hyperoxia-induced expression changes
331 most distinctive of *Ly6a*⁺ L-MSCs are illustrated in Fig. 3A. Exposure to hyperoxia was
332 associated with *Ly6a*⁺ L-MSCs - specific increase in expression of multiple pro-inflammatory
333 (*Cxcl1*, *Ccl2*), as well as pro-fibrotic and anti-angiogenic (*Timp1*, *Serpina3n*) genes (Fig. 3A,
334 Supplementary table 8). GSEA of hyperoxia-induced changes in gene expression revealed an

335 activation in inflammatory pathways, as well as decrease in pathways associated with arterial
336 development and morphogenesis (Fig. 3B, Supplementary table 9). When inspecting pathways
337 altered by hyperoxia exclusively in *Ly6a*⁺, but not *Ly6a*⁻ stromal cells, activation of cytokine and
338 chemokine signaling, cell cycle regulation, and senescence were most noticeable (Supplementary
339 fig. 2E, Supplementary table 9).

340 To further understand the faith of *Ly6a*⁺ L-MSCs in hyperoxia-induced injury, we
341 performed a cell communication analysis using the NicheNet tool, inferring hyperoxia-induced
342 cellular communications[23,28] (Fig. 3C, Supplementary fig. 6-7, Supplementary table 10).
343 *Ly6a*⁺ L-MSCs in hyperoxia-exposed lungs received signals from several cell populations,
344 including immune cells, capillary and arterial endothelial cells, mesothelial cells and *Coll3a1*⁺
345 fibroblasts (Fig. 3C). Further, we inferred genes in *Ly6a*⁺ L-MSCs most likely to be targeted by
346 the received signals (Fig. 3D). Multiple ligands, such as *ApoE*, *Il1a*, *Ifng* and *Mmp9* were
347 predicted to target the expression of pro-inflammatory, pro-fibrotic and anti-angiogenic genes
348 discussed above, including *Timp1*, *Cxcl1* and *Icam1* (Fig. 3D). Expression of these target genes
349 was elevated in *Ly6a*⁺ L-MSCs by hyperoxia exposure (Fig. 3A). Finally, ligands produced by
350 *Ly6a*⁺ L-MSCs affected multiple cell populations, including alveolar macrophages, ciliated and
351 AT2 cells, capillary and vein endothelium and other stromal populations. Among the most
352 broadly acting ligands produced by *Ly6a*⁺ L-MSCs were *Bmp4*, *Bmp5*, *Col4a1* and *Tnc* (Fig.
353 3A). Inferred target genes in receiving cells targeted by majority of these ligands included
354 *Ccnd1*, *Cdkn1a*, *Icam1* and *Hmox1* (Fig. 3E). According to FEA, expression of the L-MSC-
355 produced ligands were associated with pathways related to vessel morphogenesis, epithelial cell
356 proliferation, cell chemotaxis, and immune homeostasis and response (Supplementary fig. 2F,
357 Supplementary table 11).

358

359 **3.4 Murine LY6A⁺ L-MSCs localize to perivascular regions of the developing lung**

360 Next, we aimed to localize the *Ly6a*⁺ L-MSCs in the developing lung using FISH. L-MSCs were
361 identified as *Ly6a*⁺/*Coll4a1*⁺ cells. L-MSCs in both, normally and aberrantly-developing lungs
362 localized to perivascular regions of large vessels with more double-positive cells observed in
363 hyperoxia-exposed lungs (Fig. 4A).

364 Additionally, we aimed to validate some of the novel normoxic and hyperoxic L-MSC
365 markers as suggested by scRNA-seq analysis (Fig. 1C, Fig. 3A). *Ly6a*⁺ L-MSCs were co-stained
366 for the hyperoxia-associated markers *Timp1* and *Serpina3n* (Fig. 4B and 4C, respectively). In
367 both instances triple-positive cells were observed in the regions adjacent to large vessels
368 (highlighted by white squares in low-magnification panels). These cells were not only more
369 abundant in the lungs from BPD mice, but the expression levels of both, *Timp1* and *Serpina3n*
370 were increased in the diseased lungs (see higher-magnification panels Fig. 4B-C).

371

372 **3.5 Hyperoxia exposure does not impact clonal or differentiation potential of LY6A⁺ L-** 373 **MSCs**

374 In order to verify their progenitor cell-like properties, we isolated and studied LY6A⁺ L-MSCs
375 from healthy and hyperoxia-exposed developing mouse pups. An arrest in lung development was
376 induced by exposing newborn mouse pups to normobaric hyperoxia (85% O₂) (Fig. 5A). CD31⁻
377 /CD45⁻/EpCAM⁻/LY6A⁺ L-MSCs were isolated from seven days-old healthy (21% O₂-exposed)
378 or diseased (85% O₂-exposed) mouse pups (Fig. 5B) and examined for the hallmarks of the MSC
379 phenotype *in vitro*. While lungs of hyperoxia-exposed pups consistently yielded higher numbers
380 of LY6A⁺ L-MSCs (Fig. 5B), no differences in the appearance (Fig. 5C), differentiation capacity
381 (Fig. 5C), expression of surface markers (Fig. 5D), or clonal abilities (Fig. 5E) were observed
382 between the cells isolated from healthy and diseased animals. LY6A⁺ L-MSCs isolated from
383 both healthy and hyperoxia-exposed mice had a fibroblast-like appearance and expressed
384 classical markers of MSCs *in vitro* (Fig. 5C-D). In order to investigate their differentiation
385 capacity, LY6A⁺ L-MSCs were induced to differentiate along the osteogenic, chondrogenic, and
386 adipogenic lineages. Both normoxia and hyperoxia-derived LY6A⁺ L-MSCs produced
387 osteogenic and chondrogenic matrix (Fig. 5C). However, only a single sample of normoxia-
388 derived LY6A⁺ L-MSCs produced a small number of adipocytes, and no lipogenic
389 differentiation was observed in hyperoxia-derived LY6A⁺ L-MSCs (data not shown). Postnatal
390 hyperoxia exposure had no effect on colony-forming capacity of LY6A⁺ L-MSCs as assessed by
391 single-cell plating colony-forming assay. Both normoxia and hyperoxia-derived LY6A⁺ L-MSCs
392 produced colonies of various sizes. While larger colonies consisted of fibroblast-like spindle-
393 shaped cells, smaller colonies were formed by cells with a large cytoplasm (Fig. 5E).

394 Inconsistent differentiation capacity and colony formation might suggest a heterogeneous nature
395 of the LY6A⁺ L-MSCs population.

396

397 **3.6 Cell culture alters the gene expression profile of LY6A⁺ L-MSCs**

398 For therapeutic applications, MSCs are typically culture expanded, then frozen, over the short-,
399 or long-term and thawed prior to administration. These various steps may alter the properties of
400 the cell product. In order to understand changes in the L-MSCs expression profile induced by
401 storage and culture, we performed a scRNA-seq analysis of cultured LY6A⁺ and LY6A⁻ lung
402 stromal cells isolated from seven days-old healthy (21% O₂-exposed) or diseased (85% O₂-
403 exposed) mouse pups (Fig. 6A, Supplementary fig. 2C-D). We sequenced over 15,000 cultured
404 CD31⁻/CD45⁻/EpCAM⁻/LY6A⁻ and CD31⁻/CD45⁻/EpCAM⁻/LY6A⁺ cells and identified four
405 distinct clusters (Fig. 6A-C, Supplementary tables 12-13). While normoxia and hyperoxia-
406 derived LY6A⁻ stromal cells contributed to all four clusters, very few LY6A⁺ cells could be
407 found in clusters 2 and 3 (Fig. 6B). The presence of distinct clusters within the L-MSCs
408 population is consistent with the heterogeneous phenotype of cultured L-MSCs described above
409 (Fig. 5E). In line with this finding, the highest levels of routine MSC markers, such as *Thy1*,
410 *Eng*, *Alcam* or *Mcam*, were found in the largest cluster 0, while very little expression was seen in
411 the two smallest clusters (Fig. 6D). While still expressing routine MSC markers to some level,
412 cluster 1 was characterized by its distinct expression of *Cck*, previously found to attenuate *p53*-
413 mediated apoptosis in lung cancer [31] (Figure 3A-C). Cluster 2 was distinguished by the
414 expression of pro-adipogenic markers, such as *Igfbp2* and *Col4a1*, as well as markers of
415 myofibroblasts (*Des*) and alveolar epithelium (*Krt8* and *Prnp2*) (Fig. 6C, Supplementary table
416 13). Cluster 3 was characterized by the expression of multiple osteogenic markers, including
417 *Cryab*, *Postn* and *Ngfr*. Interestingly, the expression of both *Postn*, as well as another cluster 3
418 marker *Coll8a1*, was previously reported in BPD patients and hyperoxia-exposed developing
419 mice [32,33].

420 Next, we aimed to identify the best markers for cultured L-MSCs (Supplementary tables
421 14-18). We compared the gene expression profiles of LY6A⁺ and LY6A⁻ stromal cells
422 (Supplementary tables 15-18) and identified differentially expressed genes between normoxia-
423 and hyperoxia-derived subsets of these populations (Supplementary tables 17-18). In comparison

424 to LY6A⁻ cells, LY6A⁺ cells were characterized by high expression of *Actg2*, *Col1a2*, *Serpinf1*,
425 *Prrx1* and *Lxn*, and by low expression of smooth muscle cell (SMC) marker *Tagln2*[34], alveolar
426 progenitor marker *Tm4sf1*[35], and *Prdx6* (Fig. 6E, Supplementary tables 15-16). From these
427 markers hyperoxia exposure further specifically increased the expression of *Actg2*, and decreased
428 the expression of *Tagln2*, *Tm4sf1* and *Prdx6* in LY6A⁺ cells. Hyperoxic LY6A⁺ cells were
429 additionally distinguished by expression of *Ptn*, *Adamts5*, *Rbp*, and *Col3a1* (Fig. 6E,
430 Supplementary table 17). Expression of *Prrx1* and *Serpinf1* is known to favour an osteogenic
431 phenotype, and *Serpinf1* is known to inhibit adipogenesis[36,37].

432 In order to identify L-MSCs expression patterns maintained after cell culture and storage,
433 we next compared expression of the most promising markers of *Ly6a*⁺ L-MSCs in both, *in situ*
434 and *in vitro* datasets from cells isolated at P7 (Supplementary fig. 2G-H). This analysis revealed
435 that a large portion of the expression profile characteristic for *Ly6a*⁺ L-MSCs *in situ*
436 (Supplementary fig. 2G-H) is lost when cells are frozen and cultured, including the expression of
437 promising markers, such as *Lum*, *Ptn*, *Dcn*, or *Pi16* (Supplementary fig. 2H). Furthermore, while
438 the expression pattern of some markers, such as *Serpina3n* or *C3* persisted in cultured cells, the
439 portion of the cells expressing the gene was diminished (Fig. 7A-B). The most suitable *in situ* or
440 *in vitro*-specific identifying markers of *Ly6a*⁺ L-MSCs are depicted in Fig. 4A-B. Among the
441 most stable markers of *Ly6a*⁺ L-MSCs, resistant to changes induced by culture, were *Serpinf1*
442 and *Postn* (Fig. 7A-B, Supplementary fig. 2G-H). In order to confirm the viability of *Serpinf1* as
443 potential novel marker for L-MSCs we performed FISH in developing lungs at P14. Triple-
444 positive cells could be found in lungs of both, normoxic and hyperoxic mice (Fig. 7C). No
445 differences were apparent in *Serpinf1* expression intensity between the two groups.

446 Finally, new expression patterns arose particularly in hyperoxia-derived *Ly6a*⁺ L-MSCs
447 after cell culture. While a high *Ptn*, *Lum*, *Dcn*, *Col3a2* and *Coll4a1* expression was initially
448 characteristic of both, hyperoxia and normoxia-derived *Ly6a*⁺ L-MSCs, in cultured L-MSCs this
449 was true only for the hyperoxia-derived *Ly6a*⁺ L-MSCs (Supplementary fig. 2G-H). This
450 expression pattern denotes, that not only does the L-MSC transcriptome change in culture, but
451 that the cells isolated from lungs of diseased mice tend to retain their expression profile and,
452 potentially, progenitor-like nature longer.

453

454 **DISCUSSION**

455 Our current knowledge regarding the identity and properties of tissue resident MSCs remains
456 limited. Most studies analyse L-MSCs in culture after isolation with one, or several MSC
457 markers. However, no explicit rules regarding which markers represent the L-MSC population
458 the best exist to date. The progenitor-like characteristics of these cells have been established in
459 culture [13,14], but it is not yet known why L-MSCs fail to prevent the lung injury or restore
460 damage in the lung. While L-MSCs were previously found in bronchoalveolar lavage of BPD
461 patients [50], it is not known whether this is due to increased apoptosis and subsequent shedding
462 from the lung or is a sign of activation and proliferation of L-MSC and hence of increased
463 numbers in BPD patients. Here, we provide an extensive scRNA-seq based analysis of L-MSCs
464 in developing mouse lung, as well as in culture. We characterize the changes in transcriptomic
465 profile induced in L-MSCs by developmental age, exposure to hyperoxia, and culture. Our study
466 further provides an insight into communication between L-MSCs and other cell populations in
467 the normally and abnormally developing lung. Finally, we propose novel markers for
468 identification of L-MSCs in the developing lung.

469 The use of omics approaches to study tissue-specific MSCs *in vivo* has been previously
470 proposed [38]. In the study presented here, we utilize scRNA-seq to study L-MSCs immediately
471 after isolation (*in situ*) without confounding procedures, such as FACS, cell culture and storage,
472 and hence preserve the *in vivo* activation status of the different lung populations as much as
473 possible. We selected *Ly6a* to identify L-MSCs for 2 reasons: i) *Ly6a* is one of the most
474 commonly used L-MSC markers and its expression has been shown in specific progenitor-like
475 populations, ii) *Ly6a* was the only known MSC marker forming a visible subcluster within the
476 lung mesenchyme of early postnatal mouse pups. We identified novel markers of L-MSCs,
477 including *Lum*, *Serpinf1*, and *Dcn*. Next, we showed how the L-MSC's transcriptome changes
478 during the course of normal lung development and in hyperoxia, and explored the
479 communication between L-MSCs and other lung cell populations.

480 Hyperoxia-exposure, used as a model for BPD, was associated in *Ly6a*⁺ L-MSCs with
481 increased expression of multiple pro-inflammatory (*Cxcl1*, *Ccl2*), pro-fibrotic and anti-
482 angiogenic (*Timp1*, *Serpina3n*) genes. Similarly, increased expression of both, *Timp1* and *Ccl2*
483 was previously reported in hyperoxia-exposed rodents [39,40], and in plasma [41] or tracheal

484 aspirates (TA) [42] of BPD patients. *Timp1* expression was further increased in fibrotic foci in
485 chronic BPD [43] and in the lungs of ventilated newborns [44]. GSEA further confirmed the
486 activation of inflammatory and pro-fibrotic pathways, and a decrease in sprouting angiogenesis
487 and vessel morphogenesis in the hyperoxia-exposed developing lungs. To further explore the
488 role L-MSCs play in cell signaling during the development, we performed a cell communication
489 inference analysis. L-MSCs in healthy developing lungs received ligands secreted mainly from
490 endothelial, immune and other stromal cells. L-MSCs signalled back to the majority of lung cell
491 populations with a selected set of ligands (Fig. 2). Upon hyperoxia exposure, L-MSCs received
492 ligands primarily from immune and endothelial cells, including *Il1a*, *Mmp9*, *Ifng*, and *Fasl* (Fig.
493 3). Interestingly, multiple ligands received by L-MSCs were predicted to target the expression of
494 pro-inflammatory, pro-fibrotic and anti-angiogenic genes increased in hyperoxia-exposed L-
495 MSCs, such as *Timp1*, *Cxcl1* and *Icam1*. IFN γ and MMP9, which target the expression of both
496 *Timp1* and *Cxcl1*, were previously implicated in development of alveolar hypoplasia [45] and an
497 increased expression of IFN γ was reported in TA of BPD patients [27,46]. Development of BPD
498 was also associated with increased TA and plasma protein levels of ICAM1 [47,48]. IL1A was
499 also shown to induce an inflammatory phenotype in lung fibroblasts [49]. Additionally, *Fasl*⁺
500 immune cells were shown to induce fibroblast cell death [50,51], and its overexpression was
501 associated with alveolar apoptosis and disturbed alveolar and vascular development [52].

502 Next, we investigated how the L-MSCs' transcriptome changed due to culture and
503 storage, both necessary steps for the preparation of a cell therapeutic product. ScRNA-seq
504 analysis revealed, that following isolation, storage and culture, most L-MSCs retain the
505 expression of MSC markers, including *Ly6a*⁺. Cultured L-MSCs showed moderate ability to
506 differentiate into chondrocytes and osteoblasts. However, we observed only one instance of
507 successful differentiation along the adipogenic lineage, consistent with previous studies of L-
508 MSCs in developing rats [13]. Inconsistent differentiation capacity could be attributed to
509 heterogeneity within the L-MSC population as indicated by the variable size and morphology of
510 L-MSC-derived colonies (Fig. 5). Importantly, such heterogeneity could indicate the existence of
511 L-MSCs with varying progenitor-like capabilities, most likely impacting their therapeutic
512 efficacy. Further, more detailed characterization of different L-MSCs subpopulations might be
513 necessary in order to prepare a superior therapeutic product. ScRNA-seq revealed considerable
514 changes in the transcriptome of L-MSCs in culture, implying that the cells studied and

515 maintained *in vitro* for the purposes of therapeutic interventions are appreciably altered
516 compared to L-MSCs *in situ* (Fig. 6). Interestingly, we observed that the culture-induced
517 transcription changes are less pronounced in L-MSCs derived from hyperoxia-exposed animals.
518 This might suggest that hyperoxia primes L-MSCs to maintain certain characteristics, potentially
519 in an attempt to trigger a repair mechanism. While the organism's own resident L-MSCs fail to
520 prevent the hyperoxia-induced lung damage, a therapeutic use of injury-primed L-MSCs might
521 be more beneficial than L-MSCs from healthy individuals. Interestingly, tissue origin and
522 microenvironment were shown to significantly impact the behaviour and therapeutic efficacy of
523 MSCs [53,54]. Moreover, conditioned media from BM-MSCs exposed *ex vivo* to hyperoxia
524 exhibited superior therapeutic effects in the hyperoxia-induced rat BPD model when compared to
525 media from BM-MSCs which were not pre-conditioned [55].

526 The localization of L-MSCs in the developing lungs has not yet been described. Here, we
527 localized the L-MSC cells in the perivascular regions of both, healthy and diseased developing
528 lungs by FISH. The *Ly6a*⁺ L-MSCs in the hyperoxia-exposed lungs co-expressed *Timp1* and
529 *Serpina3e*, confirming the results of scRNA-seq analysis. Finally, as *Ly6a* is not expressed in
530 human tissues, we aimed to identify additional markers to label L-MSCs, both *in situ* and *in*
531 *vitro*. *Lum*, identified as marker of L-MSCs *in situ*, is known to be produced by MSCs. Within
532 the lung, its expression was localized to peripheral lung and vessel walls [56]. While scRNA-
533 seq revealed *Lum* as a promising L-MSCs marker *in situ*, its expression in culture was preserved
534 only in a small fraction of L-MSCs isolated from hyperoxia-exposed animals (Fig. 7A). In
535 comparison, the expression of *Serpinf1* was well preserved *in vitro*, with the expression slightly
536 increased in hyperoxic cells. Interestingly, *Serpinf1* expression was previously reported to be
537 increased in hyperoxia-exposed newborn mice and *Serpinf1*^{-/-} animals were protected from
538 hyperoxia-induced lung injury [57]. *Serpinf1* is also known as an anti-angiogenic and anti-
539 migratory marker associated with aging MSCs [57,58]. *In situ*, *Serpinf1* colocalized well with
540 *Ly6a*⁺/*Coll4a1*⁺ cells in both healthy and diseased lungs, suggesting *Serpinf1* as promising new
541 marker for L-MSCs (Fig. 7).

542 To our knowledge, this is the first detailed report studying the characteristics and
543 behaviour of L-MSC *in situ* and *in vitro*, during both health and disease. We unravelled the
544 transcriptome and cellular communication of this lung resident cell population by scRNA-seq in

545 order to mechanistically understand its endogenous repair capabilities, as well as its potential use
546 as an exogenous cell therapeutic product. In addition, we have established several markers that
547 can be used to identify L-MSC *in vitro* and *in vivo*, both in healthy and diseased lungs.
548 Additional studies will be needed to further unravel the heterogeneity of this population, as well
549 as their therapeutic capabilities.

550

551 **ACKNOWLEDGMENTS**

552 This study was supported by the Canadian Institutes of Health Research (CIHR), the German
553 Research Foundation (Deutsche Forschungsgemeinschaft), the Frederick Banting and Charles
554 Best Doctoral Scholarship, the Finnish Foundation for Pediatric Research, the Finnish Sigrid
555 Juselius Foundation, the Canadian Lung Association - Breathing as One, and the Molly Towel
556 Perinatal Research Foundation.

557

558 **DISCLOSURE OF POTENTIAL CONFLICT OF INTERESTS**

559 The authors declare no conflicts of interest, financially or otherwise.

560

561 **AUTHOR CONTRIBUTIONS**

562 IM: Conception and design, collection and assembly of data, data analysis and interpretation,
563 manuscript writing, final approval of manuscript. DPC: Collection and assembly of data, data
564 analysis and interpretation, manuscript writing, final approval of manuscript. CCD: Collection
565 and assembly of data, data analysis and interpretation, manuscript writing, final approval of
566 manuscript. FL: Collection and assembly of data, data analysis and interpretation, manuscript
567 writing, final approval of manuscript. MH: Collection and assembly of data, final approval of
568 manuscript. SMH: Collection and assembly of data, final approval of manuscript. SZ: Collection
569 and assembly of data, final approval of manuscript. OC: Financial support, administrative
570 support, final approval of manuscript. BCV: Financial support, administrative support, final
571 approval of manuscript. BT: Conception and design, financial support, administrative support,
572 final approval of manuscript.

573

574 **DATA AVAILABILITY STATEMENT**

575

576 **REFERENCES**

- 577 1 Warburton D. Overview of Lung Development in the Newborn Human. *Neonatology*
578 2017;111:398–401.
- 579 2 Thébaud B, Goss KN, Laughon M, et al. Bronchopulmonary dysplasia. *Nat Rev Dis Primers*
580 2019;5:78.
- 581 3 Wong PM, Lees AN, Louw J, et al. Emphysema in young adult survivors of moderate-to-severe
582 bronchopulmonary dysplasia. *European Respiratory Journal* 2008;32:321–328.
- 583 4 Fawke J, Lum S, Kirkby J, et al. Lung Function and Respiratory Symptoms at 11 Years in Children
584 Born Extremely Preterm: The EPICure Study. *Am J Respir Crit Care Med* 2010;182:237–245.
- 585 5 O’Reilly M, Möbius MA, Vadivel A, et al. Late Rescue Therapy with Cord-Derived Mesenchymal
586 Stromal Cells for Established Lung Injury in Experimental Bronchopulmonary Dysplasia. *Stem Cells and*
587 *Development* 2020;29:364–371.
- 588 6 van Haaften T, Byrne R, Bonnet S, et al. Airway Delivery of Mesenchymal Stem Cells Prevents
589 Arrested Alveolar Growth in Neonatal Lung Injury in Rats. *Am J Respir Crit Care Med* 2009;180:1131–
590 1142.
- 591 7 Sutsko RP, Young KC, Ribeiro A, et al. Long-term reparative effects of mesenchymal stem cell
592 therapy following neonatal hyperoxia-induced lung injury. *Pediatr Res* 2013;73:46–53.
- 593 8 Pierro M, Ionescu L, Montemurro T, et al. Short-term, long-term and paracrine effect of human
594 umbilical cord-derived stem cells in lung injury prevention and repair in experimental
595 bronchopulmonary dysplasia. *Thorax* 2013;68:475–484.
- 596 9 Augustine S, Cheng W, Avey MT, et al. Are all stem cells equal? Systematic review, evidence
597 map, and meta-analyses of preclinical stem cell-based therapies for bronchopulmonary dysplasia. *STEM*
598 *CELLS Translational Medicine* 2020;9:158–168.
- 599 10 Aslam M, Baveja R, Liang OD, et al. Bone Marrow Stromal Cells Attenuate Lung Injury in a
600 Murine Model of Neonatal Chronic Lung Disease. *Am J Respir Crit Care Med* 2009;180:1122–1130.
- 601 11 Collins JJP, Thébaud B. Progenitor cells of the distal lung and their potential role in neonatal lung
602 disease: Progenitor Cells of The Distal Lung. *Birth Defects Research Part A: Clinical and Molecular*
603 *Teratology* 2014;100:217–226.
- 604 12 Ushakumary MG, Riccetti M, Perl AT. Resident interstitial lung fibroblasts and their role in
605 alveolar stem cell niche development, homeostasis, injury, and regeneration. *STEM CELLS Transl Med*
606 2021:sctm.20-0526.
- 607 13 Collins JJP, Lithopoulos MA, dos Santos CC, et al. Impaired Angiogenic Supportive Capacity and
608 Altered Gene Expression Profile of Resident CD146⁺ Mesenchymal Stromal Cells Isolated from
609 Hyperoxia-Injured Neonatal Rat Lungs. *Stem Cells and Development* 2018;27:1109–1124.
- 610 14 Lama VN, Smith L, Badri L, et al. Evidence for tissue-resident mesenchymal stem cells in human
611 adult lung from studies of transplanted allografts. *J Clin Invest* 2007;117:989–996.

- 612 15 Rolandsson Enes S, Andersson Sjöland A, Skog I, et al. MSC from fetal and adult lungs possess
613 lung-specific properties compared to bone marrow-derived MSC. *Sci Rep* 2016;6:29160.
- 614 16 Deng M, Li J, Gan Y, et al. Changes in the number of CD31⁺;CD45⁺;Sca-1⁺ cells and Shh
615 signaling pathway involvement in the lungs of mice with emphysema and relevant effects of acute
616 adenovirus infection. *COPD* 2017;Volume 12:861–872.
- 617 17 Gong X, Sun Z, Cui D, et al. Isolation and characterization of lung resident mesenchymal stem
618 cells capable of differentiating into alveolar epithelial type II cells: Isolation and characterization of LR-
619 MSCs. *Cell Biol Int* 2014;38:405–411.
- 620 18 Shi C, Cao X, Chen X, et al. Intracellular surface-enhanced Raman scattering probes based on TAT
621 peptide-conjugated Au nanostars for distinguishing the differentiation of lung resident mesenchymal
622 stem cells. *Biomaterials* 2015;58:10–25.
- 623 19 McQualter JL, Brouard N, Williams B, et al. Endogenous Fibroblastic Progenitor Cells in the Adult
624 Mouse Lung Are Highly Enriched in the Sca-1 Positive Cell Fraction. *Stem Cells* 2009;27:623–633.
- 625 20 McQualter JL, Yuen K, Williams B, et al. Evidence of an epithelial stem/progenitor cell hierarchy
626 in the adult mouse lung. *Proceedings of the National Academy of Sciences* 2010;107:1414–1419.
- 627 21 Salaets T, Gie A, Jimenez J, et al. Local pulmonary drug delivery in the preterm rabbit: feasibility
628 and efficacy of daily intratracheal injections. *American Journal of Physiology-Lung Cellular and Molecular
629 Physiology* 2019;316:L589–L597.
- 630 22 McGinnis CS, Patterson DM, Winkler J, et al. MULTI-seq: sample multiplexing for single-cell RNA
631 sequencing using lipid-tagged indices. *Nat Methods* 2019;16:619–626.
- 632 23 Hurskainen M, Mižíková I, Cook DP, et al. Single cell transcriptomic analysis of murine lung
633 development on hyperoxia-induced damage. *Nat Commun* 2021;12:1565.
- 634 24 Butler A, Hoffman P, Smibert P, et al. Integrating single-cell transcriptomic data across different
635 conditions, technologies, and species. *Nat Biotechnol* 2018;36:411–420.
- 636 25 Hafemeister C, Satija R. Normalization and variance stabilization of single-cell RNA-seq data
637 using regularized negative binomial regression. *Genome Biol* 2019;20:296.
- 638 26 Liberzon A, Birger C, Thorvaldsdóttir H, et al. The Molecular Signatures Database Hallmark Gene
639 Set Collection. *Cell Systems* 2015;1:417–425.
- 640 27 Aghai ZH, Saslow JG, Mody K, et al. IFN- γ and IP-10 in tracheal aspirates from premature infants:
641 Relationship with bronchopulmonary dysplasia. *Pediatr Pulmonol* 2013;48:8–13.
- 642 28 Browaeys R, Saelens W, Saeys Y. NicheNet: modeling intercellular communication by linking
643 ligands to target genes. *Nat Methods* 2020;17:159–162.
- 644 29 Malinowski M, Pietraszek K, Perreau C, et al. Effect of Lumican on the Migration of Human
645 Mesenchymal Stem Cells and Endothelial Progenitor Cells: Involvement of Matrix Metalloproteinase-14.
646 *PLoS ONE* 2012;7:e50709.

- 647 30 Li L-F, Chu P-H, Hung C-Y, et al. Lumican Regulates Ventilation-Induced Epithelial-Mesenchymal
648 Transition Through Extracellular Signal-Regulated Kinase Pathway. *Chest* 2013;143:1252–1260.
- 649 31 Han Y, Su C, Yu D, et al. Cholecystokinin attenuates radiation-induced lung cancer cell apoptosis
650 by modulating p53 gene transcription. *Am J Transl Res* 2017;9:638–646.
- 651 32 Bozyk PD, Bentley JK, Popova AP, et al. Neonatal Periostin Knockout Mice Are Protected from
652 Hyperoxia-Induced Alveolar Simplification. *PLoS ONE* 2012;7:e31336.
- 653 33 Mohamed WAW, Niyazy WH, Mahfouz AA. Angiopoietin-1 and Endostatin Levels in Cord Plasma
654 Predict the Development of Bronchopulmonary Dysplasia in Preterm Infants. *Journal of Tropical*
655 *Pediatrics* 2011;57:385–388.
- 656 34 Shudo Y, Cohen JE, Goldstone AB, et al. Isolation and trans-differentiation of mesenchymal
657 stromal cells into smooth muscle cells: Utility and applicability for cell-sheet engineering. *Cytherapy*
658 2016;18:510–517.
- 659 35 Zacharias WJ, Frank DB, Zepp JA, et al. Regeneration of the lung alveolus by an evolutionarily
660 conserved epithelial progenitor. *Nature* 2018;555:251–255.
- 661 36 Yu S, Li P, Li B, et al. RelA promotes proliferation but inhibits osteogenic and chondrogenic
662 differentiation of mesenchymal stem cells. *FEBS Lett* 2020;594:1368–1378.
- 663 37 Gattu AK, Swenson ES, Iwakiri Y, et al. Determination of mesenchymal stem cell fate by pigment
664 epithelium-derived factor (PEDF) results in increased adiposity and reduced bone mineral content.
665 *FASEB j* 2013;27:4384–4394.
- 666 38 Sipp D, Robey PG, Turner L. Clear up this stem-cell mess. *Nature* 2018;561:455–457.
- 667 39 Hosford GE, Fang X, Olson DM. Hyperoxia Decreases Matrix Metalloproteinase-9 and Increases
668 Tissue Inhibitor of Matrix Metalloproteinase-1 Protein in the Newborn Rat Lung: Association with
669 Arrested Alveolarization. *Pediatr Res* 2004;56:26–34.
- 670 40 Kumar VHS, Lakshminrusimha S, Kishkurno S, et al. Neonatal hyperoxia increases airway
671 reactivity and inflammation in adult mice: Neonatal Hyperoxia and AHR in Mice. *Pediatr Pulmonol*
672 2016;51:1131–1141.
- 673 41 Schulz CG, Sawicki G, Lemke RP, et al. MMP-2 and MMP-9 and Their Tissue Inhibitors in the
674 Plasma of Preterm and Term Neonates. *Pediatr Res* 2004;55:794–801.
- 675 42 Fulton CT, Cui TX, Goldsmith AM, et al. Gene Expression Signatures Point to a Male Sex-Specific
676 Lung Mesenchymal Cell PDGF Receptor Signaling Defect in Infants Developing Bronchopulmonary
677 Dysplasia. *Sci Rep* 2018;8:17070.
- 678 43 Dik WA, de Krijger RR, Bonekamp L, et al. Localization and Potential Role of Matrix
679 Metalloproteinase-1 and Tissue Inhibitors of Metalloproteinase-1 and -2 in Different Phases of
680 Bronchopulmonary Dysplasia. *Pediatr Res* 2001;50:761–766.
- 681 44 De Paepe ME, Greco D, Mao Q. Angiogenesis-related gene expression profiling in ventilated
682 preterm human lungs. *Experimental Lung Research* 2010;36:399–410.

- 683 45 Harijith A, Choo-Wing R, Cataltepe S, et al. A Role for Matrix Metalloproteinase 9 in IFN γ -
684 Mediated Injury in Developing Lungs: Relevance to Bronchopulmonary Dysplasia. *Am J Respir Cell Mol*
685 *Biol* 2011;44:621–630.
- 686 46 Hikino S, Ohga S, Kinjo T, et al. Tracheal aspirate gene expression in preterm newborns and
687 development of bronchopulmonary dysplasia: TAF cell gene expression predicting BPD. *Pediatrics*
688 *International* 2012;54:208–214.
- 689 47 Ballabh P, Kumari J, Krauss AN, et al. Soluble E-Selectin, Soluble L-Selectin and Soluble ICAM-1 in
690 Bronchopulmonary Dysplasia, and Changes With Dexamethasone. *PEDIATRICS* 2003;111:461–468.
- 691 48 Kojima T, Sasai M, Kobayashi Y. Increased soluble ICAM-1 in tracheal aspirates of infants with
692 bronchopulmonary dysplasia. *The Lancet* 1993;342:1023–1024.
- 693 49 Suwara MI, Green NJ, Borthwick LA, et al. IL-1 α released from damaged epithelial cells is
694 sufficient and essential to trigger inflammatory responses in human lung fibroblasts. *Mucosal Immunol*
695 2014;7:684–693.
- 696 50 Nareznoi D, Konikov-Rozenman J, Petukhov D, et al. Matrix Metalloproteinases Retain Soluble
697 FasL-mediated Resistance to Cell Death in Fibrotic-Lung Myofibroblasts. *Cells* 2020;9:411.
- 698 51 Predescu SA, Zhang J, Bardita C, et al. Mouse Lung Fibroblast Resistance to Fas-Mediated
699 Apoptosis Is Dependent on the Baculoviral Inhibitor of Apoptosis Protein 4 and the Cellular FLICE-
700 Inhibitory Protein. *Front Physiol* 2017;8.
- 701 52 De Paepe ME, Gundavarapu S, Tantravahi U, et al. Fas-Ligand-Induced Apoptosis of Respiratory
702 Epithelial Cells Causes Disruption of Postcanalicular Alveolar Development. *The American Journal of*
703 *Pathology* 2008;173:42–56.
- 704 53 Abreu SC, Rolandsson Enes S, Dearborn J, et al. Lung inflammatory environments differentially
705 alter mesenchymal stromal cell behavior. *American Journal of Physiology-Lung Cellular and Molecular*
706 *Physiology* 2019;317:L823–L831.
- 707 54 Islam D, Huang Y, Fanelli V, et al. Identification and Modulation of Microenvironment Is Crucial
708 for Effective Mesenchymal Stromal Cell Therapy in Acute Lung Injury. *Am J Respir Crit Care Med*
709 2019;199:1214–1224.
- 710 55 Waszak P, Alphonse R, Vadivel A, et al. Preconditioning Enhances the Paracrine Effect of
711 Mesenchymal Stem Cells in Preventing Oxygen-Induced Neonatal Lung Injury in Rats. *Stem Cells and*
712 *Development* 2012;21:2789–2797.
- 713 56 Dolhnikoff M, Morin J, Roughley PJ, et al. Expression of Lumican in Human Lungs. *Am J Respir*
714 *Cell Mol Biol* 1998;19:582–587.
- 715 57 Chetty A, Bennett M, Dang L, et al. Pigment Epithelium–Derived Factor Mediates Impaired Lung
716 Vascular Development in Neonatal Hyperoxia. *Am J Respir Cell Mol Biol* 2015;52:295–303.
- 717 58 Liang H, Hou H, Yi W, et al. Increased expression of pigment epithelium-derived factor in aged
718 mesenchymal stem cells impairs their therapeutic efficacy for attenuating myocardial infarction injury \ddagger .
719 *European Heart Journal* 2013;34:1681–1690.

720 **Figure 1. Gene expression profile of *Ly6a*⁺ L-MSCs during late lung development. (A)** Six clusters of
721 stromal cells were previously identified in developing lungs. In the dataset re-analyzed here mice were
722 exposed to room air (21% O₂) or hyperoxia (85%O₂) from P1 onwards and lungs were harvested at P3, P7
723 and P14. UMAP plot depicting the distribution of lung stromal cells based on the developmental age and
724 oxygen exposure. **(B)** UMAP plots showing the expression of *Ly6a* mRNA (left panel) within the lung
725 stroma and new cluster identities, including the *Ly6a*⁺ L-MSCs. **(C)** Heatmap of top ten most differentially
726 expressed genes across stromal clusters depicted in panel (B). **(D)** Dotplot depicting expression of
727 routine MSC markers in lung stromal populations. **(E)** Relative contribution of *Ly6a*⁺ and *Ly6a*⁻ cells in
728 developing lung stroma at P3, P7 and P14. n = 6 animals/group. Data are presented as means ± SD.
729 Statistical analyses were performed with GraphPad Prism 8.0 and the presence of potential statistical
730 outliers was determined by Grubbs' test. Significance was evaluated by multiple unpaired Student's *t*-
731 test with Holm-Šidák correction for *Ly6a*⁺ and *Ly6a*⁻ cells separately. *P* values < 0.05 were considered
732 significant and are depicted. **(F)** Dotplot depicting the expression of most differentially expressed genes
733 in *Ly6a*⁺ L-MSCs during normal lung development. **(G)** Dotplot depicting the expression of genes that are
734 differentially expressed specifically in *Ly6a*⁺ L-MSCs and not in other lung stromal clusters during normal
735 lung development. **(H)** Selected developmental age-associated signalling pathways in the *Ly6a*⁺ L-MSC
736 cluster identified by gene set enrichment analysis (GSEA). All terms are significantly enriched (adjusted
737 p-value < 0.05). Normalized enrichment scores (NES) values were computed by gene set enrichment
738 analysis on fold change-ranked genes. Expression values in Heatmap represent Z-score-transformed
739 log(TP10k+1) values. Expression levels in Dotplots and UMAP plots are presented as log(TP10k+1)
740 values. Log(TP10k+1) corresponds to log-transformed UMIs per 10k.

741

742 **Figure 2. Age-associated gene expression and signalling in the developing *Ly6a*⁺ L-MSCs. (A)** Circos plot
743 showing inferred cell communications between *Ly6a*⁺ L-MSCs and other populations in the developing
744 mouse lung. Cell communications associated with increasing developmental age are depicted. Cell types
745 in the top right correspond to receiver populations with the largest expression changes in response to
746 increasing age. These cell types are connected to the sender cell types expressing ligands predicted to
747 promote this response. Ligands expressed by the same cell population are coloured the same. **(B)**
748 Heatmap depicting predicted target genes for ligands most likely to be received by normally developing
749 *Ly6a*⁺ L-MSC population as indicated in **(A)**. The intensity of expression is indicated as specified by the
750 colour legend. **(C)** Heatmap depicting predicted target genes for ligands sent by *Ly6a*⁺ L-MSC population

751 in normally developing lungs as indicated in **(A)**. The intensity of expression is indicated as specified by
752 the colour legend.

753

754 **Figure 3. Hyperoxia-induced gene expression and signalling in the developing *Ly6a*⁺ L-MSCs. (A)**

755 Dotplot depicting the expression of markers specifically altered by hyperoxia exposure in *Ly6a*⁺ and *Ly6a*⁻
756 cells in the developing mouse lung. **(B)** Selected hyperoxia-regulated signalling pathways in the *Ly6a*⁺ L-

757 MSC cluster identified by gene set enrichment analysis (GSEA). All terms are significantly enriched
758 (adjusted p-value < 0.05). Normalized enrichment scores (NES) values were computed by gene set

759 enrichment analysis on fold change-ranked genes. **(C)** Circos plot showing inferred cell communications
760 between *Ly6a*⁺ L-MSCs and other populations in the developing mouse lung. Cell communications

761 induced by exposure to hyperoxia are depicted. Cell types in the top right correspond to receiver
762 populations with the largest expression changes in response to hyperoxia. These cell types are

763 connected to the sender cell types expressing ligands predicted to promote this response. Ligands
764 expressed by the same cell population are coloured the same. **(D)** Heatmap depicting predicted target

765 genes for ligands most likely to be received by *Ly6a*⁺ L-MSC population in hyperoxia as indicated in **(C)**.
766 The intensity of expression is indicated as specified by the colour legend. **(E)** Heatmap depicting

767 predicted target genes for ligands sent by *Ly6a*⁺ L-MSC population in hyperoxia as indicated in **(C)**. The
768 intensity of expression is indicated as specified by the colour legend.

769

770 **Figure 4. Identification of *Ly6a*⁺ L-MSCs in the developing lung. (A)** Fluorescent RNA *in situ* hybridization

771 showing localization of L-MSCs identified by the co-expression of *Ly6a* (white) and *Col14a1* (green) in
772 lungs of room air (21% O₂) or hyperoxia (85%O₂)-exposed developing mice. Scale bar = 200µm for low-

773 magnification (5×, top panels) windows, 50µm for higher-magnification (40×, bottom left panels)
774 windows, and 20µm for high-magnification (63×, bottom right panels) windows. Four 14-days old

775 animals/group were analysed. Expression levels in Dotplot are presented as log(TP10k+1) values.
776 Log(TP10k+1) corresponds to log-transformed UMIs per 10k. **(B)** Fluorescent RNA *in situ* hybridization

777 showing co-expression of *Ly6a* (white), *Col14a1* (green), and *Timp1* (pink) in lungs of room air (21% O₂)
778 or hyperoxia (85%O₂)-exposed developing mice. Scale bar = 200µm for low-magnification (5×, top left)

779 windows, 50µm for higher-magnification (40×, top right) windows, and 20µm for high-magnification
780 (63×, bottom panels) windows. Four 14-days old animals/group were analysed. **(C)** Fluorescent RNA *in*

781 *situ* hybridization showing co-expression of *Ly6a* (white), *Col14a1* (green), and *Serpina3n* (pink) in lungs
782 of room air (21% O₂) or hyperoxia (85%O₂)-exposed developing mice. Scale bar = 200µm for low-
783 magnification (5×, top left) windows, 50µm for higher-magnification (40×, top right) windows, and 20µm
784 for high-magnification (63×, bottom panels) windows. Four 14-days old animals/group were analysed.

785

786 **Figure 5. Characterization of LY6A⁺ L-MSCs in normal and impaired mouse lung development. (A)**

787 Mouse pups were exposed to room air (21% O₂, grey) or hyperoxia (85%O₂, blue) from P1 onwards. Mice
788 were harvested on postnatal day (P)7. Representative histological sections from lungs developing in 21%
789 O₂ or 85% O₂. Lung morphometry was quantified by the mean linear intercept (MLI) measurement. n = 7
790 animals/group. Scale bar = 100µm. **(B)** LY6A⁺ L-MSCs were identified by flow cytometry as CD45-AF647⁻
791 /CD31-FITC/CD326(EPCAM)-PeCy7⁻/LY6A(SCA1)-BV421⁺ cells and their proportion in lung homogenates
792 was quantified. n = 8-9 animals/group. **(C)** Representative images of undifferentiated LY6A⁺ L-MSCs and
793 LY6A⁺ L-MSCs differentiated towards osteogenic and chondrogenic lineages and stained with Alizarin
794 Red S or Alcian Blue, respectively. Scale bar = 250µm. Experiments were performed in quadruplets. **(D)**
795 Expression of routine MSCs surface markers in cultured LY6A⁺ L-MSCs isolated from room air (21% O₂,
796 grey bars) or hyperoxia-exposed (85%O₂, purple bars) developing pups as determined by flow
797 cytometry. n = 3-4 animals/group. **(E)** Quantification and representative images of colony formation of
798 cultured LY6A⁺ L-MSCs isolated from room air (21% O₂, grey bars) or hyperoxia-exposed (85%O₂, purple
799 bars). n = 4 animals/group. Scale bar =100µm. All data are presented as means ± SD. Statistical analyses
800 were performed with GraphPad Prism 8.0. The presence of potential statistical outliers was determined
801 by Grubbs' test. Significance was evaluated by unpaired Student's *t*-test for analysis in panels (A) and
802 (B), and by multiple unpaired Student's *t*- test with Holm-Šidák correction in panels (D) and (E). *P* values
803 < 0.05 were considered significant and are depicted.

804

805 **Figure 6. Gene expression profile of cultured normoxia and hyperoxia-derived LY6A⁺ L-MSCs. (A)**

806 and LY6A⁻ stromal cells isolated from lungs of room air (21% O₂) or hyperoxia (85%O₂)-exposed
807 developing mice were frozen, cultured and sequenced at passage 3. n = 3 animals/group. scRNA-seq
808 identified four clusters of cultured LY6A⁺ and LY6A⁻ stromal cells. **(B)** Relative distribution of room air
809 (21% O₂) or hyperoxia (85%O₂)-derived LY6A⁺ and LY6A⁻ cells to the four different clusters. n = 3
810 animals/group. **(C)** Heatmap of top ten most differentially expressed genes across clusters depicted in

811 panel (A). **(D)** Violin plots depicting expression of routine MSC markers in cultured stromal populations.
812 **(E)** Dotplot depicting expression of oxygen-specific markers in LY6A⁺ and LY6A⁻ cultured lung stromal
813 cells. Expression values in Heatmap and violin plots represent Z-score-transformed log(TP10k+1) values.
814 Expression levels in Dotplot and UMAP plot are presented as log(TP10k+1) values. Log(TP10k+1)
815 corresponds to log-transformed UMIs per 10k.

816

817 **Figure 7. Identification of novel markers for *in situ* and cultured Ly6a⁺ L-MSCs.**

818 **(A)** Identifying markers were first established in the *in situ*, or cultured Ly6a⁺ and Ly6a⁻ lung stromal cells
819 based on Supplementary figures 1G-H. Dotplot depicts the expression levels of those markers, most
820 suitable for identification of Ly6a⁺ and Ly6a⁻ lung stromal cells *in situ* in normoxic or hyperoxic animals at
821 P7. **(B)** Identifying markers were first established in the *in situ*, or cultured Ly6a⁺ and Ly6a⁻ lung stromal
822 cells based on Supplementary figures 1G-H. Dotplot depicts the expression levels of those markers, most
823 suitable for identification of normoxia-derived and hyperoxia-derived LY6A⁺ and LY6A⁻ lung stromal cells
824 in culture. **(C)** Fluorescent RNA *in situ* hybridization showing co-expression of Ly6a (white), Col14a1
825 (green), and Serpinf1 (pink) in lungs of room air (21% O₂) or hyperoxia (85%O₂)-exposed developing
826 mice. Scale bar = 200µm for low-magnification (5×, top left) windows, 50µm for higher-magnification
827 (40×, top right) windows, and 20µm for high-magnification (63×, bottom panels) windows. Four 14-days
828 old animals/group were analysed.

829

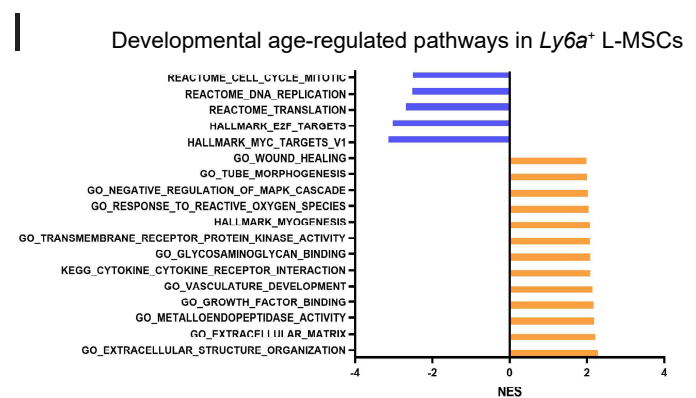
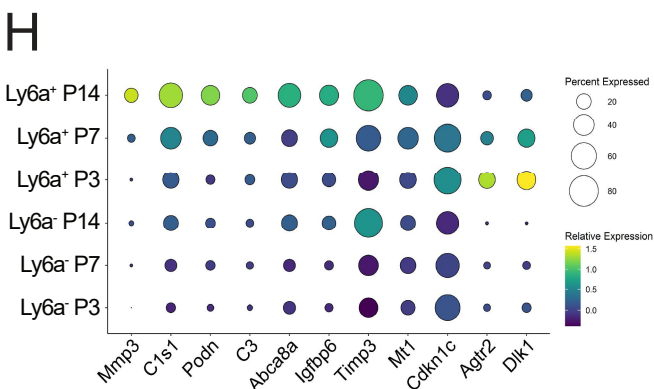
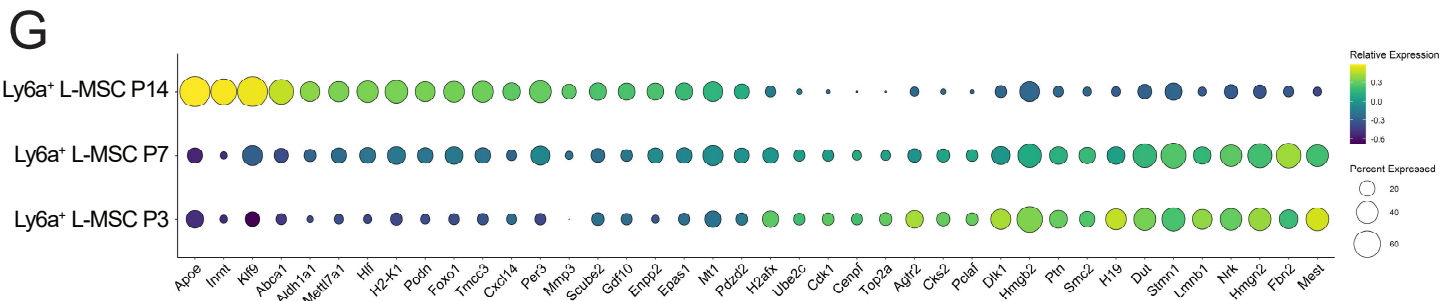
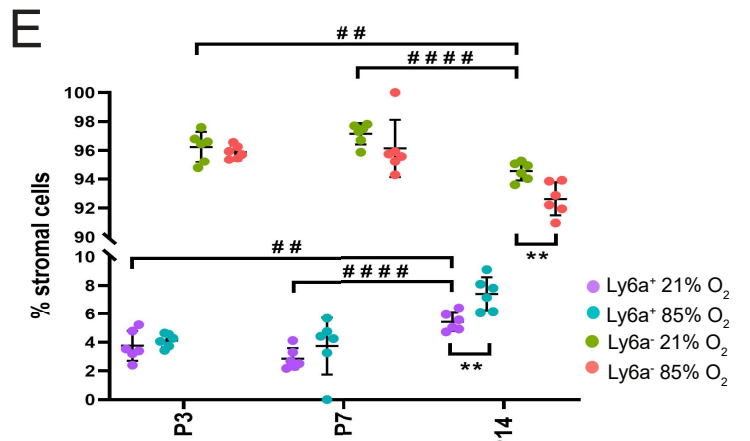
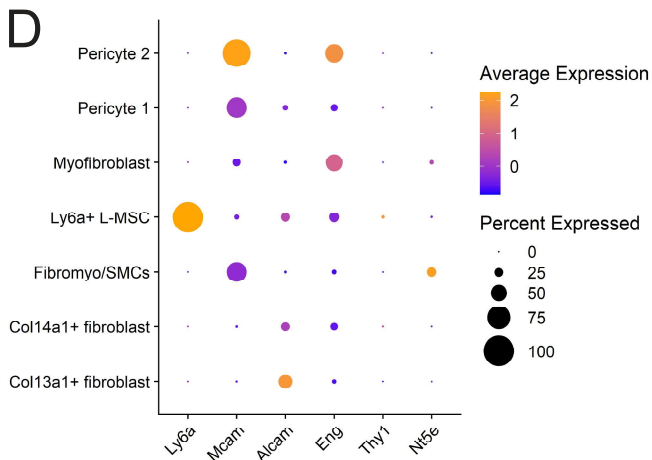
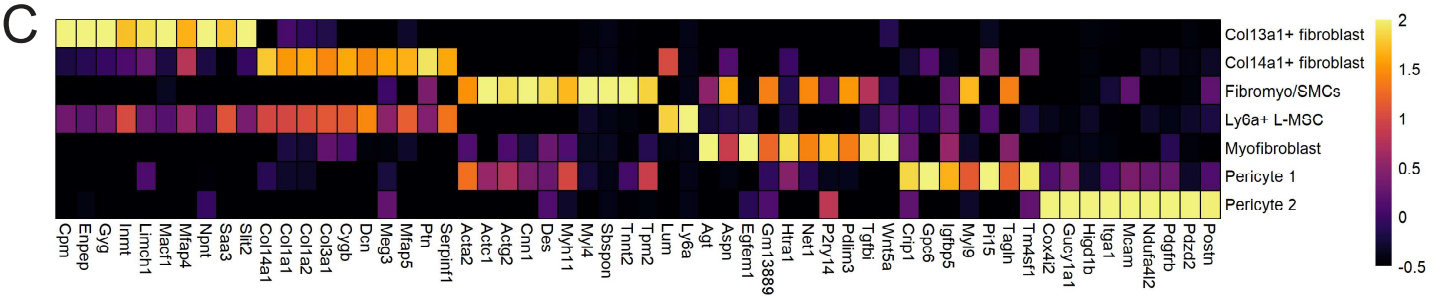
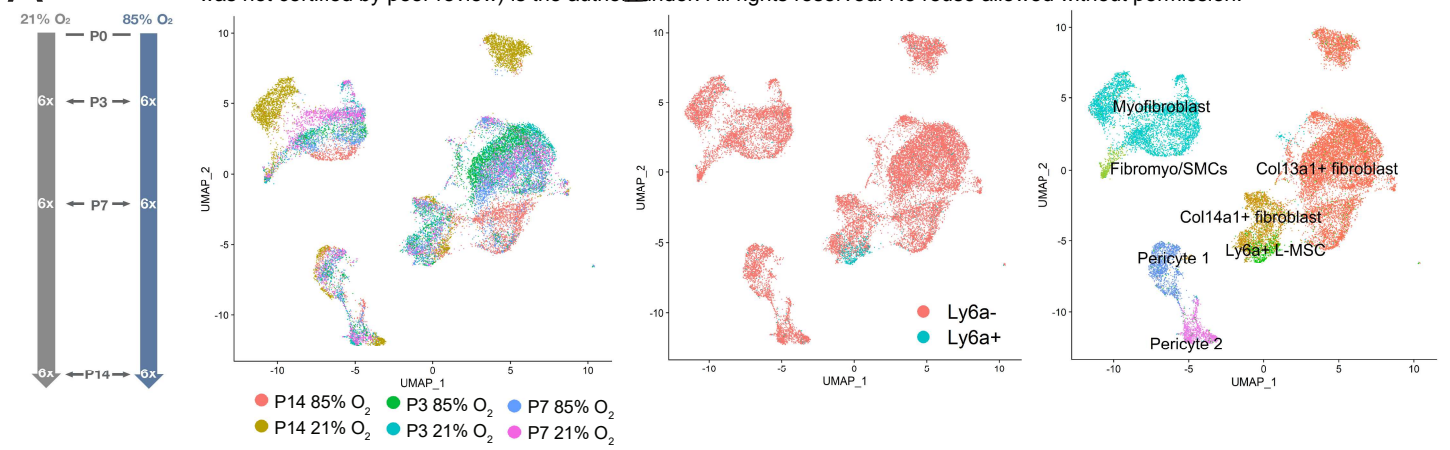
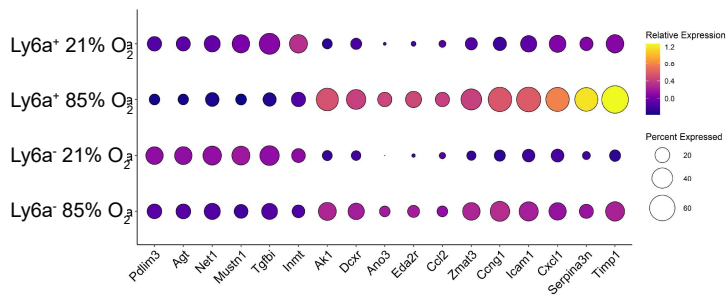
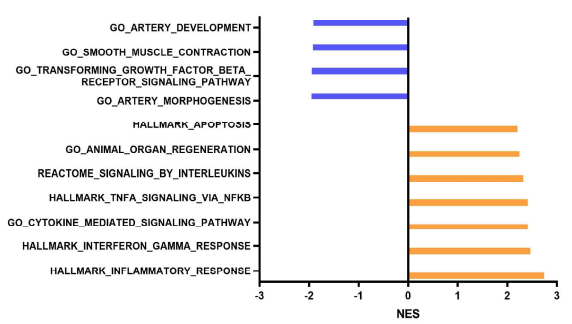


Figure 1

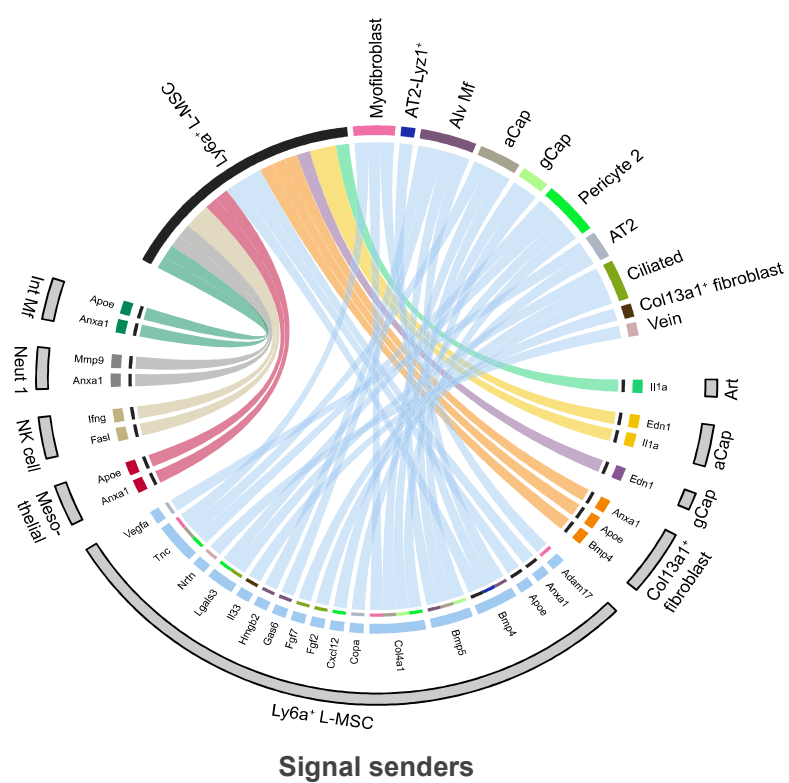
A



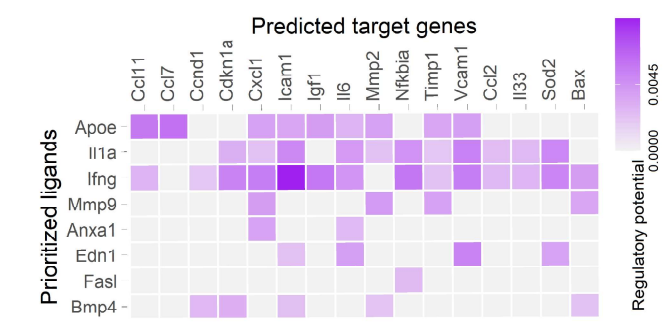
B



C



D



E

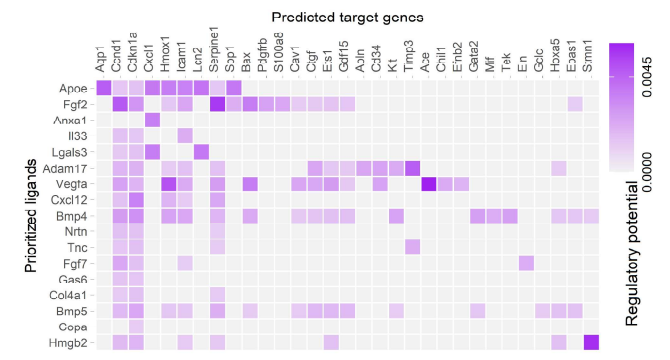
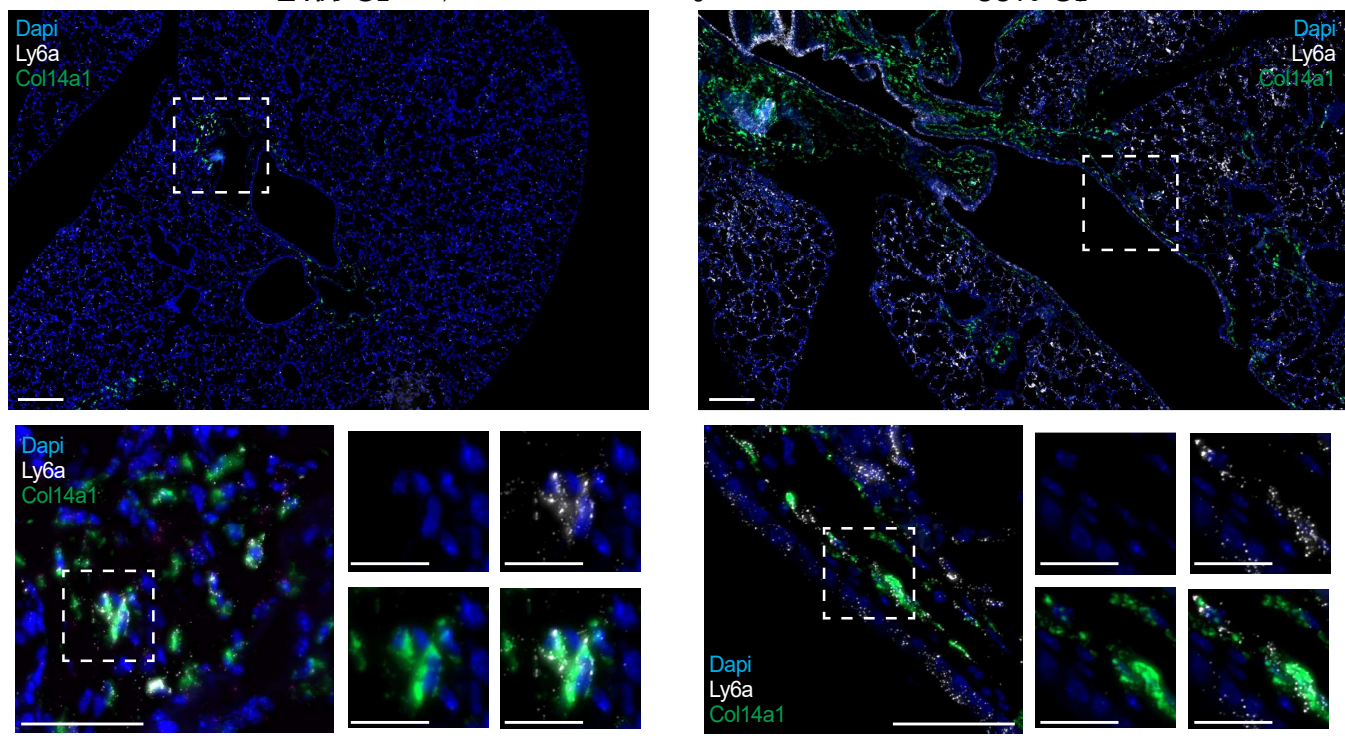
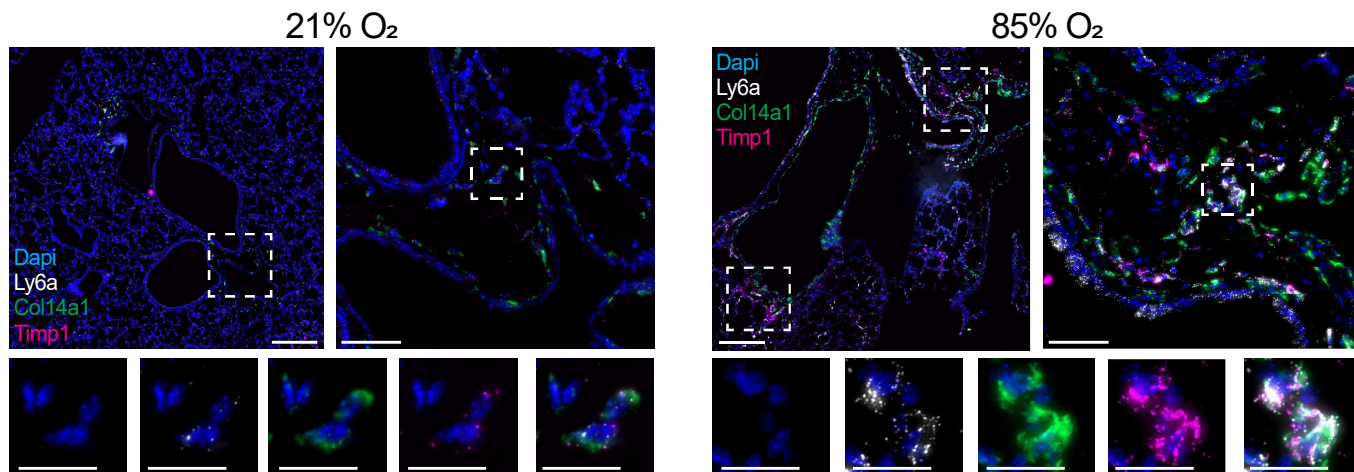


Figure 3

A



B



C

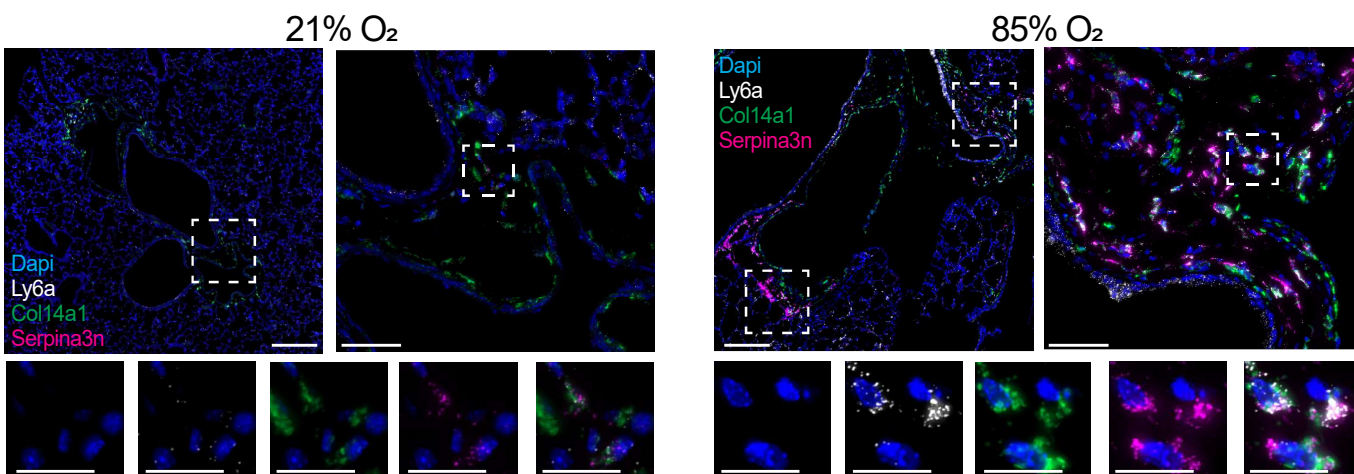


Figure 4

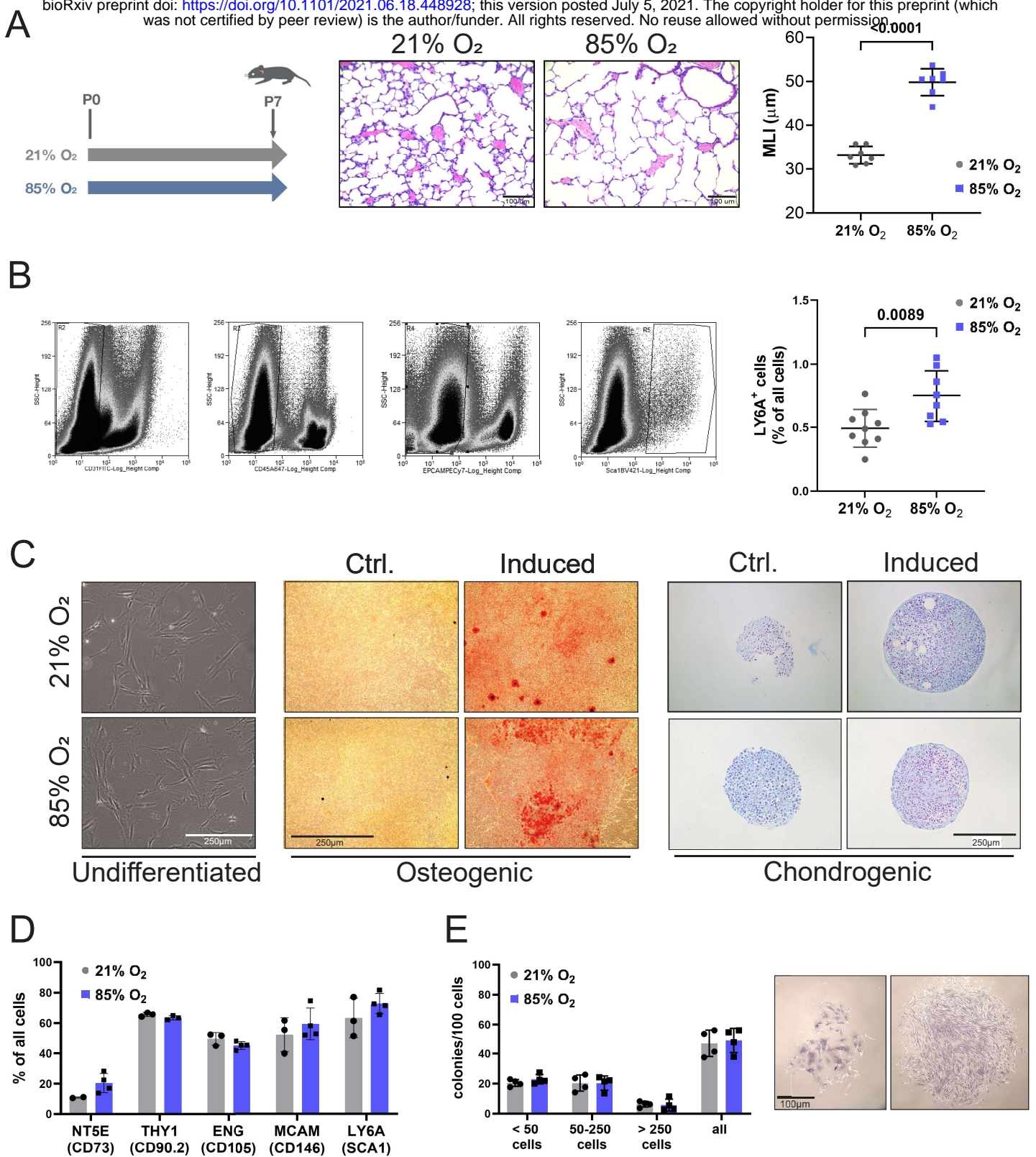
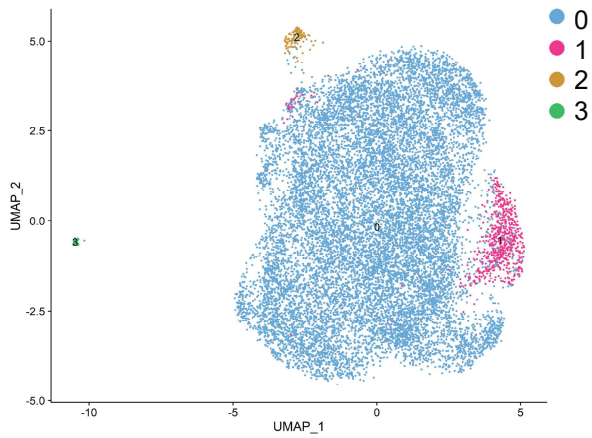


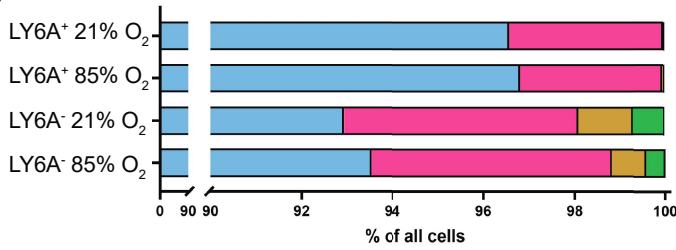
Figure 5

A

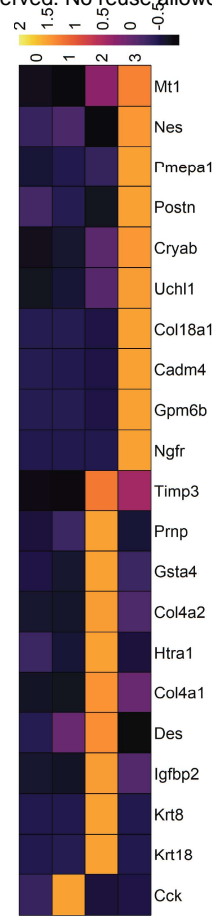
| Cell population | 21% O ₂ | 85% O ₂ | |
|----------------------------------|--------------------|--------------------|------|
| LR-MSC (LY6A ⁺) | 2579 | 2565 | 5144 |
| Lung stroma (LY6A ⁻) | 6084 | 3793 | 9877 |



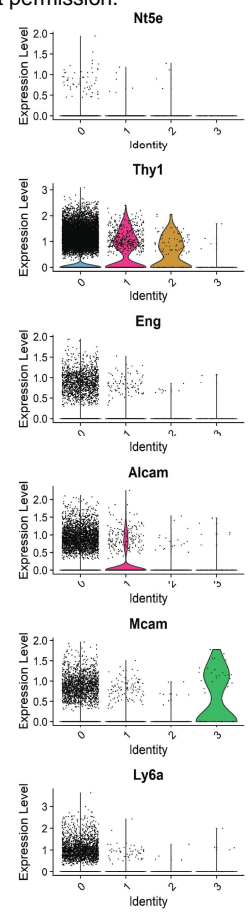
B



C



D



E

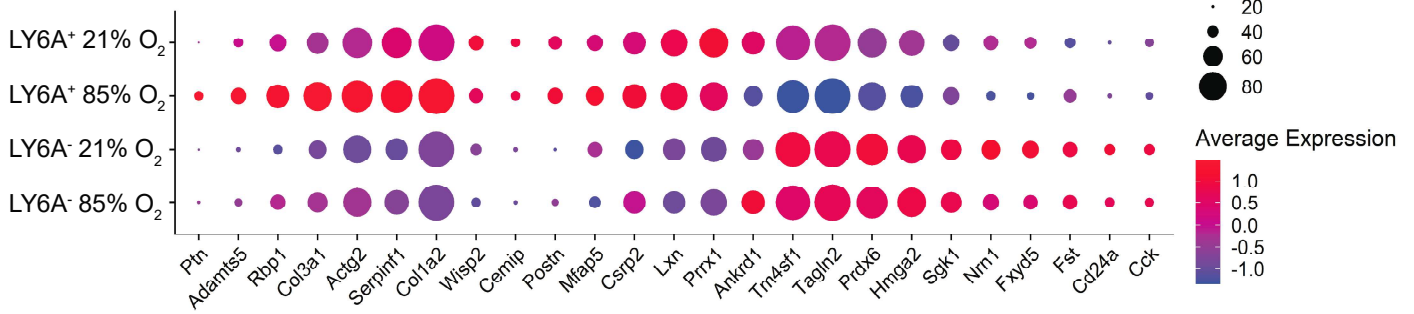
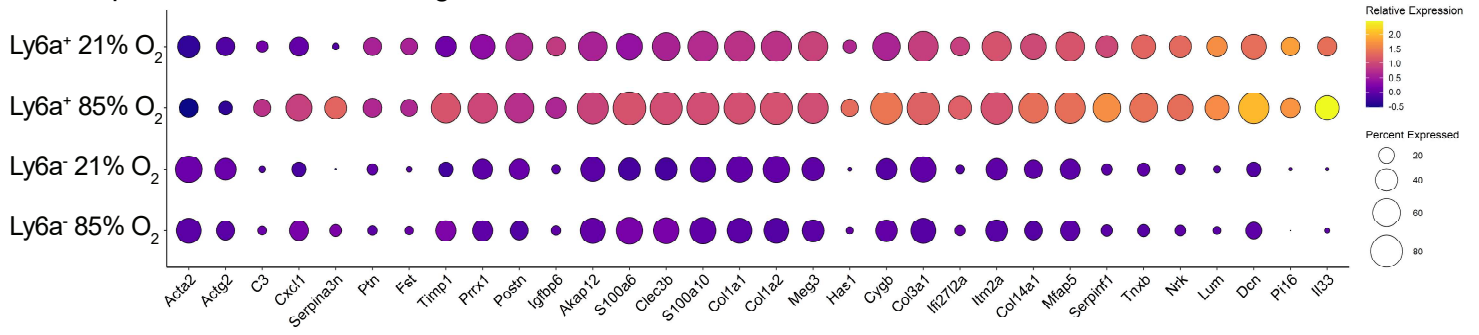
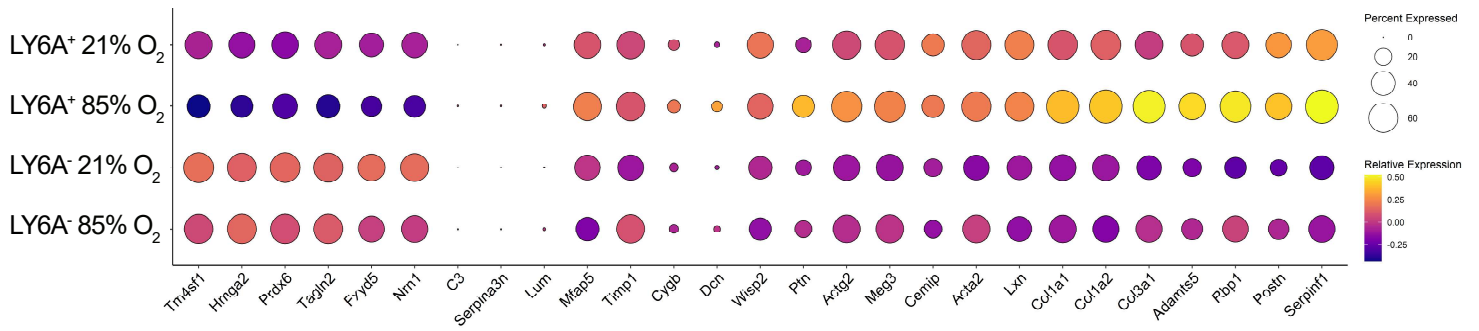


Figure 6

A Expression in the *in situ* lung stromal cells



B Expression in the cultured lung stromal cells



C

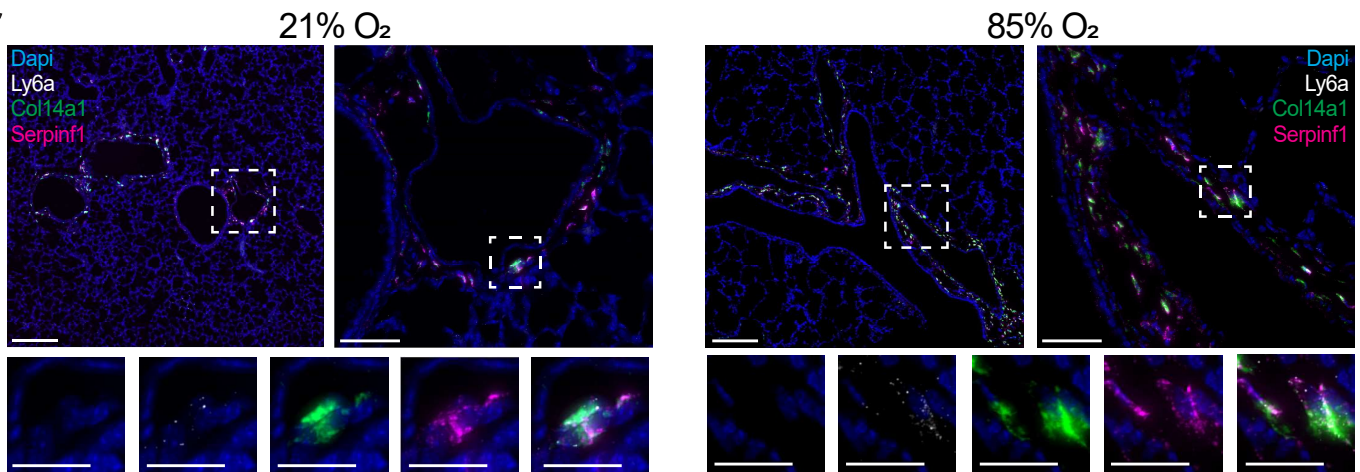


Figure 7